ResearchGate

See discussions, stats, and author profiles for this publication at: https://www.researchgate.net/publication/291217932

Geology and mineralogical zonation of the Olympic Dam iron oxide Cu–U–Au–Ag deposit, South Australia

Article · December 2012

CITATIONS
151

READS
9,193

3 authors, including:



Kathy Ehrig
BHP Billiton Limited
184 PUBLICATIONS **2,773** CITATIONS
SEE PROFILE



Vadim S. Kamenetsky
University of Tasmania
475 PUBLICATIONS **18,618** CITATIONS
SEE PROFILE

Some of the authors of this publication are also working on these related projects:

Project Plumes: Melt inclusions study: View project

Project The origin and evolution of intrusive and extrusive carbonatites View project

All content following this page was uploaded by Vadim S. Kamenetsky on 17 January 2019.

The user has requested enhancement of the downloaded file.



www.segweb.org

Special Publication Number 16

Geology and Genesis of Major Copper Deposits and Districts of the World: A Tribute to Richard H. Sillitoe

Jeffrey W. Hedenquist, Michael Harris, and Francisco Camus, Editors

© 2012 Society of Economic Geologists, Inc.
Special Publication 16, pp. 237–267

Chapter 11

Geology and Mineralogical Zonation of the Olympic Dam Iron Oxide Cu-U-Au-Ag Deposit, South Australia

Kathy Ehrig,[†,1] Jocelyn McPhie,[2] and Vadim Kamenetsky[2]

[1] *BHP Billiton Olympic Dam, 55 Grenfell St, Adelaide, South Australia 5000, Australia*

[2] *ARC Centre of Excellence in Ore Deposits and School of Earth Sciences, University of Tasmania, Hobart, Tasmania 7001, Australia*

Abstract

Olympic Dam is a supergiant Fe oxide Cu-U-Au-Ag deposit that is also strongly enriched in a wide range of elements, including F, S, C, As, Ba, Bi, Cd, Co, Cr, Fe, In, Mo, Nb, Ni, P, Pb, Sb, Se, Sn, Sr, Te, V, W, Y, Zn, and rare earth elements (REE). The deposit contains more than 90 minerals. Mineralization was associated with intense, texturally destructive hematite and sericite alteration and brecciation of the primary host rock units, including Roxby Downs Granite, bedded clastic facies rocks, and mafic-ultramafic dikes. Based on comprehensive geological, geochemical, and mineralogical data sets collected during a deposit-scale resource delineation and sterilization drilling program (2003–2008), compiled with historical geological data and interpretations, we quantify geochemical and mineralogical associations and distribution patterns.

The granite-derived elements (Al, Be, Ca, Hf, K, Li, Mg, Mn, Na, Rb, Si, Th, Ti, and Zr) are negatively correlated with Fe, whereas the hydrothermal elements (Ag, As, Au, Ba, Bi, Cd, Co, CO_2, Cr, Cu, F, Fe, In, Mo, Nb, Ni, P, Pb, S, Sb, Se, Sn, Sr, Te, U, V, W, Y, Zn, and REE) are positively correlated; the ore and gangue minerals are also correlated with Fe abundance. There is a strong spatial association of Cu, U_3O_8, Au, and Ag. From the periphery inward and upward from depth toward the deposit center, the most significant zones are as follows: (1) reduced Fe oxide alteration (magnetite-apatite-siderite-chlorite-quartz) → oxidized Fe oxide alteration (hematite-sericite-fluorite) → hematite-quartz-barite alteration, (2) siderite → fluorite → barite, (3) sphalerite → galena → pyrite → chalcopyrite → bornite → chalcocite → nonsulfide, and (4) distal or paragenetically early (?) base metal-poor (Mo-W-Sn-As-Sb) → base metal-rich (Cu-Pb-Zn) minerals → sulfide-barren hematite-quartz-barite breccia in the deposit center. Spatially isolated remnants of advanced argillic alteration (sericite + quartz ± Al-OH) have been defined for the first time. Progressive Fe oxide addition to, and sericite replacement of the primary host rocks produced distinctive, albeit complex, hydrothermally altered and mineralized zones in the Olympic Dam deposit.

Introduction

The Olympic Dam iron-oxide copper-gold (IOCG)-uranium-silver deposit, located approximately 520 km north-northwest of Adelaide, South Australia, was discovered by Western Mining Corporation (WMC) in July 1975. Olympic Dam currently contains the world's largest published uranium, fifth largest copper, and third largest gold resource (9,576 Mt at 0.82 % Cu, 0.26 kg/t U_3O_8, 0.31 g/t Au, 1.39 g/t Ag; Table 1)[1]; production commenced in mid-1988. Ore is mined via sublevel open stoping, and is processed through to final products (copper cathode, uranium ore concentrate, and gold and silver bullion) onsite via a fully integrated processing plant consisting of a sulfide concentrator, sulfuric acid leaching and solvent extraction, smelting, electrorefining and electrowinning circuits. BHP Billiton acquired WMC Resources in July 2005 and commenced studies to evaluate future mining and processing options for Olympic Dam.

Between 2003 and 2008, approximately 1,000 diamond holes (~448,000 m) were drilled from surface in the eastern two-thirds of the deposit, with an additional ~1,600 diamond holes drilled from underground in the western one-third of the deposit. The primary purpose of the surface drilling during this period was to increase the size of the resource and upgrade it in the eastern two-thirds of the deposit that is potentially suitable for open pit mining. Sterilization drilling for infrastructure purposes was also part of the program. Geological-geotechnical logging and assaying were completed on all diamond core, and the analytical pulps from all drill core samples (~600,000) drilled prior to 1997 were re-assayed for an expanded suite of elements. Ore characterization and geometallurgical testing were also conducted, which involved the measurement of modal mineralogy on approximately 10,000 samples. This extensive data collection program was driven by the need to develop predictive models which could quantify mineral abundances and metallurgical response across the entire deposit. The drill core assay data (~1.6 M samples), mineralogical data and predictive models were used to produce three-dimensional (3-D) geological models and geostatistically estimated resource models for 26 elements, bulk dry density, and 15 minerals. These new data have significantly enhanced our understanding of the metallurgical

[†] Corresponding author: e-mail, Kathy.J.Ehrig@bhpbilliton.com

[1] The Mineral Resource information is based on information compiled by Shane O'Connell, a member of the AusIMM and a full-time employee of BHP Billiton. Mr. O'Connell has sufficient experience that is relevant to this style of mineralization and type of deposit under consideration, and to the activity that he is undertaking, to qualify as a Competent Person as defined in the 2004 Edition of the "Australasian Code for Reporting of Exploration Results, Mineral Resources and Ore Reserves" (The JORC Code). Mr. O'Connell verifies that this report is based on and fairly reflects the Mineral Resource information in the supporting documentation and agrees with the form and context of the information presented.

TABLE 1. Olympic Dam Mineral Resources as of June 30, 2012

	Mt	Cu (wt %)	U_3O_8 (kg/t)	Au (g/t)	Ag (g/t)
Measured	1,474	1.03	0.30	0.35	1.95
Indicated	4,843	0.84	0.27	0.34	1.50
Inferred	3,259	0.70	0.23	0.25	0.98
Total Resources	9,576	0.82	0.26	0.31	1.39

From http://www.bhpbilliton.com/home/investors/reports/Documents/2012/BHPBillitonAnnualReport2012.pdf

properties, alteration characteristics, controls on mineralization, and architecture of the Olympic Dam deposit.

In this paper we discuss new aspects of the geology, hydrothermal alteration and mineralization at Olympic Dam based on the comprehensive, deposit-scale geochemical and mineralogical data sets, and geological data from the 2003 to 2008 major drilling campaign, and our geological and mineralogical observations and interpretations. We present improved definitions of the spatial extent of hydrothermal alteration and mineralization, previously undocumented evidence for advanced argillic alteration (sericite + quartz + Al-OH minerals) and occurrences of Mo-W-Sn-As-Sb and Zn-Pb mineralization, and discuss the spatial extent of the bedded sedimentary facies rocks described by McPhie et al. (2011b).

Only the salient deposit characteristics that are necessary to describe the geology and mineralogical zonation patterns will be presented here. Published accounts of the discovery history, early resource delineation drilling, geology, brecciation, hydrothermal alteration and mineralization at Olympic Dam are given in Roberts and Hudson (1983), O'Driscoll (1985), Oreskes and Einaudi (1990, 1992), Reeve (1990a, b), Reeve et al. (1990), Woodall (1994), Haynes et al. (1995), and Johnson and Cross (1995).

Sampling, Analytical Methods, Drill Hole Database, and Geological Resource Models

Approximately 10,000 diamond drill holes (~2.1 Mm) have been drilled for geological purposes into the basement (see below) at Olympic Dam since discovery. Drilling was carried out both from surface (735,000 m) and underground (1.365 Mm). Surface drilling included a combination of percussion or diamond drilling through ~320 m of undeformed and unaltered, flat-lying sedimentary rocks (referred to as the cover sequence), followed by diamond drilling from just above the basement (i.e., rocks which lie below the base of the cover sequence). Samples from the cover sequence were logged, with limited assaying. The basement diamond core was logged and all core is sampled and assayed at 1-m intervals; all underground drill core was logged and sampled at 2.5 m intervals, whereas core which was devoid of mineralization is sampled at 5-m intervals. Prior to 1996, underground drill core was sampled at 1- and 6-m intervals in mineralized and unmineralized rock, respectively. All diamond core was photographed and magnetic susceptibility measurements completed prior to sampling, and bulk dry density is measured on all samples via a water immersion method prior to crushing and pulverizing; the core remaining after sampling is stored onsite.

Since 1997, all drill core samples has been assayed for the same suite of elements using a combination of four-acid digestion and inductively coupled plasma-optical emission spectroscopy (ICP-OES) for Cu, Ag, As, Co, Ni, Pb, and Zn; ICP-OES for Ba, Al, Ca, Ce, Fe, K, La, Mg, Mn, Na, P, Si, Sr, Ti, Y, and Zr; lithium metaborate/tetraborate fusion and inductively coupled plasma-mass spectroscopy (ICP-MS) for U_3O_8, Bi, Sb, and Mo; induction furnace-infrared spectrometry (IF-IS) for CO_2 and S; and fire assay-flame atomic absorption spectrometry (FA-AAS) for Au. Samples assayed prior to 1997 were re-assayed to include the above suite of elements. Analytical pulps from all assayed samples are also archived onsite.

Modal mineralogy was measured via Mineral Liberation Analyzer (MLA; Gu, 2003) on approximately 10,000 samples of 15-m-long quarter-core composites collected on a widely spaced grid across the deposit; quantitative XRD (X-ray diffraction) mineralogy was also completed on a 6,000 sample subset. Assaying for an expanded suite of elements, in addition to the above listed (Be, Cl, Cr, Cs, Dy, Er, Eu, F, FeO, Ga, Gd, Hf, Ho, In, Li, Lu, Nb, Nd, Pd, Pr, Pt, Rb, Sc, Se, Sm, Sn, Ta, Tb, Te, Th, Tl, Tm, V, W, Yb, ^{204}Pb, ^{206}Pb, ^{207}Pb, ^{208}Pb) was also completed on the 10,000 samples analyzed by MLA via methods suitable for Olympic Dam mineralogy and concentration ranges. Drill locations and the above data are stored in a relational database for resource and geological modeling.

Resource block models were generated for Cu, U_3O_8, Au, Ag, S, Ba, Al, As, Ca, Ce, Co, Fe, K, La, Mg, Mn, Mo, Na, Ni, P, Pb, Si, Sr, Ti, Zn, Zr, bulk dry density, hematite, quartz, sericite, orthoclase, chlorite, siderite, fluorite, barite, pyrite, chalcopyrite, bornite, and chalcocite using a combination of ordinary, indicator, and multiple indicator kriging estimation techniques (S. O'Connell, pers. commun., 2008). Three-dimensional geological models were produced by wire-framing rock types logged in drill core in combination with the resource models.

Regional Geological Setting of Olympic Dam

Olympic Dam is located on the eastern edge of the Gawler Craton, which comprises late Archean, Paleoproterozoic, and Mesoproterozoic successions. Late Archean complexes are mainly restricted to the northern (Mulgathing Complex) and southern (Sleaford Complex) margins of the craton. Archean metavolcanic units do occur ~60 km northwest of Olympic Dam (Reid et al., 2009). In the southern and eastern Gawler Craton, the Paleoproterozoic succession includes the Hutchison Group (2000–1850 Ma; quartzite, metacarbonate, and iron formations), intruded by the Donington Suite granites (1855–1845 Ma; Hand et al., 2007). Along the eastern edge of the Gawler Craton, the younger but still Paleoproterozoic metasedimentary Wallaroo Group and equivalents (~1760 Ma) are widespread. Major deformation and metamorphic events affected the Archean (Sleafordian orogeny) and Paleoproterozoic (Kimban orogeny) units of the Gawler Craton (Hand et al., 2007).

The most voluminous and conspicuous part of the Mesoproterozoic succession is the ~1590 Ma Gawler silicic large igneous province (SLIP; McPhie et al., 2008; Allen et al., 2008). This province is dominated by largely undeformed subaerial volcanic units of the Gawler Range Volcanics (Giles, 1988; Blissett et al., 1993; Allen and McPhie, 2002; Allen et

al., 2003, 2008). The lower Gawler Range Volcanics includes mafic and felsic lavas, and felsic ignimbrites and other pyroclastic facies (Giles, 1988; Blissett et al., 1993; Roache et al., 2000; Allen et al., 2008). The upper Gawler Range Volcanics are dominated by three large-volume rhyolite lavas (Allen and McPhie, 2002; Allen et al., 2008). The Gawler SLIP also includes mainly granitoid intrusions of the Hiltaba Suite (~1598–1583 Ma; Fanning et al., 1988; Flint, 1993), and was locally affected by the Kararan (1565-1540 Ma) orogeny, involving reactivation of faults and shear zones in the northern and western Gawler Craton.

The eastern Gawler Craton in the region of Olympic Dam is overlain by the Mesoproterozoic Pandurra Formation composed of continental-derived sedimentary rocks (Cowley, 1991); the age of the Pandurra Formation is estimated to be 1424 ± 51 (Rb-Sr; Fanning et al., 1983). The Pandurra Formation is not preserved at Olympic Dam but elsewhere nearby it is overlain by Neoproterozoic to Cambrian sedimentary rocks of the Stuart Shelf (Preiss, 1993). East of the Torrens Hinge zone, the sedimentary formations belong to the Adelaide geosyncline and they become markedly thicker.

The Gairdner Dyke Swarm comprises a 180- to 250-km-wide NW-striking group of mafic-ultramafic dikes which intruded the eastern and northern Gawler Craton and the Pandurra Formation at ~825 Ma (Zhao and McCulloch, 1993; Zhao et al., 1994; Hoatson et al., 2008).

Geology of the Olympic Dam Deposit

The Olympic Dam deposit occurs entirely within the Olympic Dam Breccia Complex, a name first used by Reeve et al. (1990) to describe all breccias and related rock units associated with the Olympic Dam ore environment. This complex (Fig. 1) is hosted within the Roxby Downs Granite, part of the Hiltaba Suite (Creaser, 1989). Other minor rock units (Fig. 2) within the Olympic Dam Breccia Complex include felsic and mafic-ultramafic volcanic rocks (Gawler Range Volcanics) as well as a thick succession of bedded clastic facies rocks. A post-brecciation and -mineralization cover sequence overlies the Roxby Downs Granite and Olympic Dam Breccia Complex and consists of ~320 m of Neoproterozoic to Cambrian sedimentary rocks.

Pre-brecciation lithologies

Roxby Downs Granite: The Roxby Downs Granite is an undeformed, pink, medium- to coarse-grained, equigranular granite containing approximately 45 wt % alkali feldspar, 30% quartz, 20% sodic plagioclase, and minor biotite and amphibole with accessory to trace amounts of igneous magnetite, sphene, apatite, zircon, allanite, fluorite, ankerite, synchysite, and uranothorite (Table 2). Diagnostic properties of unaltered Roxby Downs Granite include the presence of biotite, K_2O/Na_2O ratios of ~5.5:3.5, magnetic susceptibility range of ~25 to 50 × 10^{-3} SI units, and bulk dry density of ~2.65 to 2.70 g/cm^3.

Felsic volcanic units: Remnants of feldspar-phyric felsic lavas occur as porphyritic felsic fragments in parts of the Olympic Dam Breccia Complex and in some beds in the bedded clastic facies.

Bedded clastic facies: Intervals up to 350 m thick of bedded clastic facies occur in the Olympic Dam Breccia Complex, mainly near the top of the breccia complex and immediately below the unconformity but also at deeper levels. Contacts with the hematite-rich breccia are faulted or appear to be gradational, but the intense alteration makes interpretation difficult. Bedded clastic facies rocks differ markedly from the hematite-rich breccia, having well-defined planar beds and overall finer grain size.

Bedded clastic facies comprise four main facies associations distinguished by composition, grain size, and bed forms: (1) laminated, green sandstone and mudstone, (2) well-bedded,

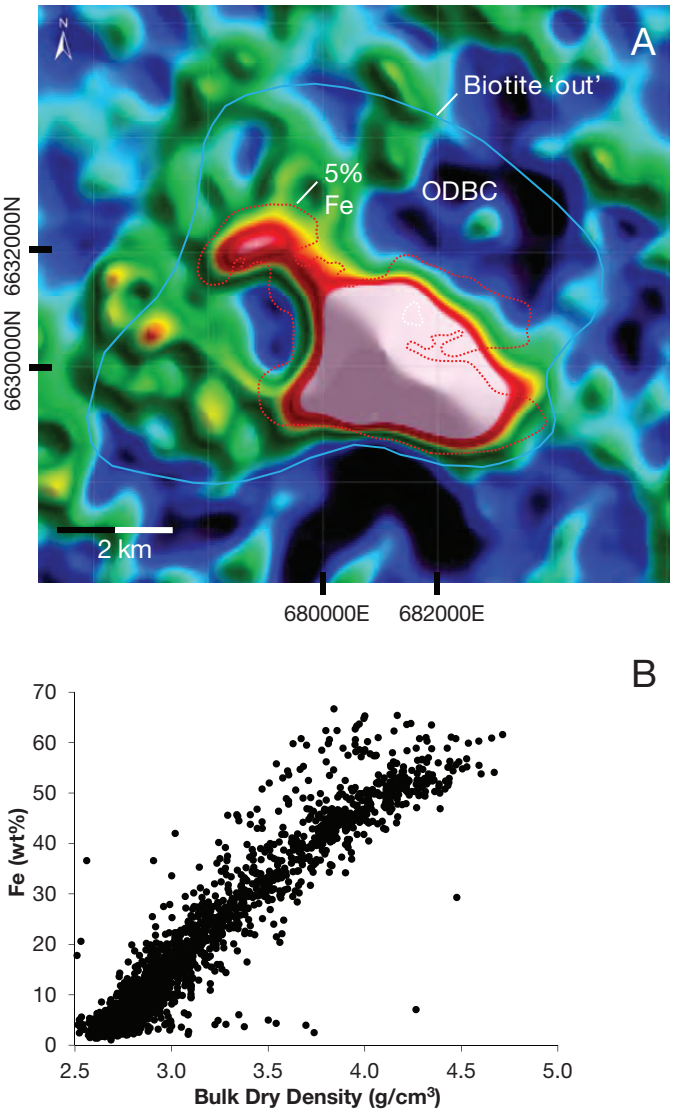


FIG. 1. A. Residual Falcon gravity image of the immediate area surrounding the Olympic Dam deposit. The residual gravity values range from –0.35 mGal (dark blue) through to +0.35 mGal (pink). Unaltered (presence of igneous biotite) Roxby Downs Granite occurs outside of the blue line (at –350m RL). The Olympic Dam Breccia Complex (ODBC) occurs on the inside of the blue line. Altered Roxby Downs Granite can occur outside this line, although igneous biotite does not occur inside. The inner red line is the 5 wt % Fe contour (at –350 mRL). B. Bulk dry density vs. whole-rock Fe wt %. Data are from a subset of the 10,000-sample MLA data set. This relationship along with the residual gravity supports the interpretation that iron metasomatism increases rapidly toward the center of the deposit. The coordinates are referenced to GDA94 / MGA zone 53.

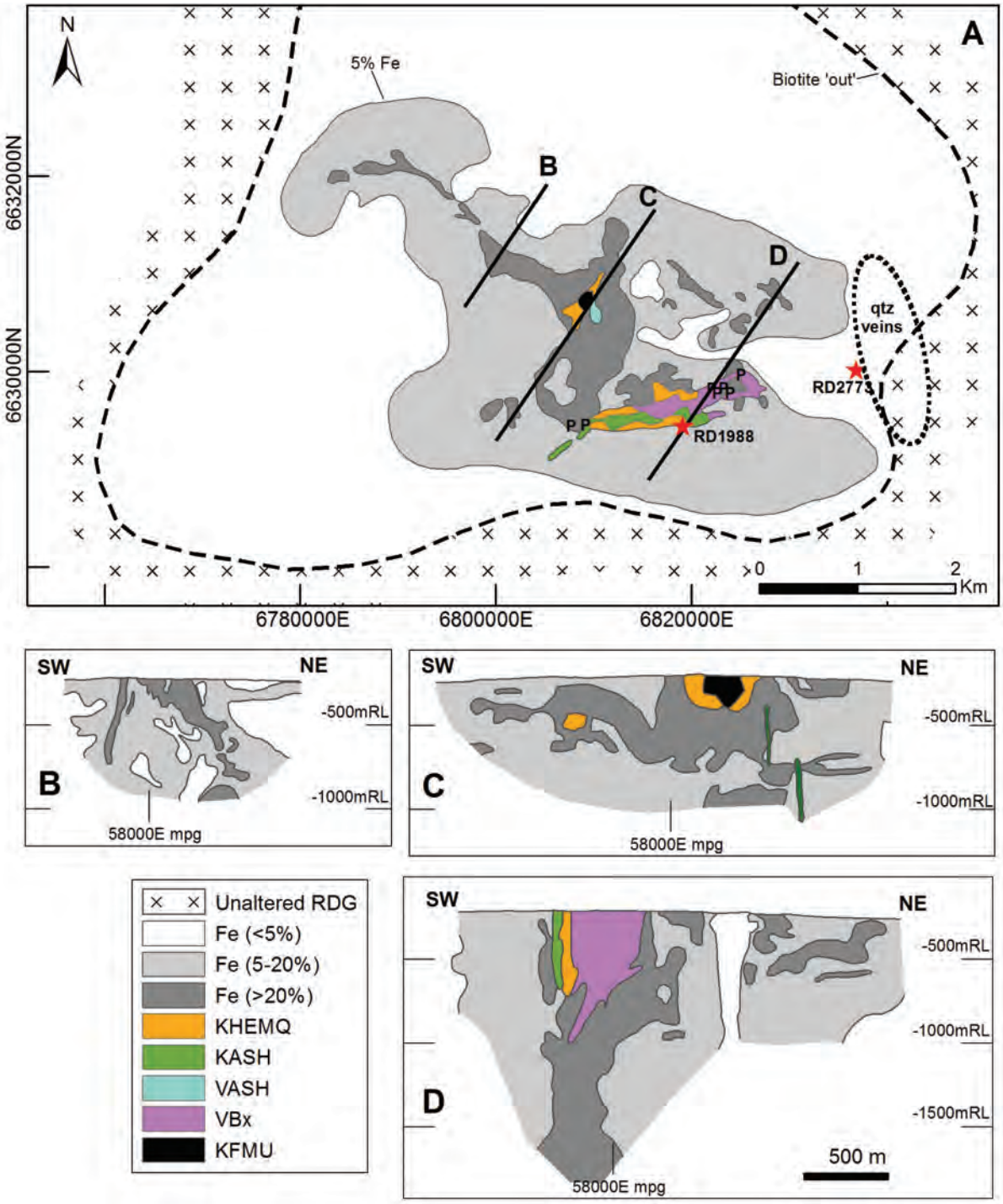


FIG. 2. Simplified geologic map at –350 mRL (A) and cross sections (B-D) of the Olympic Dam Breccia Complex, showing the distribution of unaltered Roxby Downs Granite, outer limits of significant brecciation and iron metasomatism (5 wt % Fe contour), granite-rich breccias (5–20% Fe), hematite-rich breccias (>20% Fe), chlorite-bearing, laminated sandstone and mudstone (KASH), well-bedded, hematite-rich sandstone, mudstone, and conglomerate-breccia (KHEMQ), thinly laminated, very hematite-rich mudstones (VASH), polymictic volcanic conglomerate (KFMU), hematite-rich breccias consisting of porphyritic felsic volcanic clasts (VBx). The locations of drill holes with picrite lavas are labeled with "P". The stippled area shows the locations of thick quartz veins. The locations of RD1988 and RD2773 (mentioned in the text) are also shown.

hematite-rich sandstone, mudstone, and conglomerate-breccia, (3) thinly laminated, hematite-rich mudstones, and (4) minor but thick beds of polymict volcanic conglomerate-breccia.

The laminated, green sandstone and mudstone facies are mainly composed of chlorite-altered ferromagnesian grains, sericite-altered feldspar grains, mafic volcanic fragments,

TABLE 2. Chemical Analysis of Roxby Downs Granite, Minor Units, and Various Breccias[1]

		RDG n = 49	RDG-ser alt n = 68	KASH n = 111	KHEMQ n = 71	VASH n = 92	KFMU n = 43	VBx n = 155	Picrite n = 20	Picrite n = 11	Alt dike n = 17	Dol n = 17	HEMQ n = 35	HEMQ n = 91	Bx-Mo n = 63	Bx-Zn n = 55	Bx-cp n = 30	Bx-mt n = 30
SiO_2	wt%	69.64	69.95	53.31	46.51	12.32	56.05	50.03	34.15	41.15	34.33	48.35	12.32	21.16	28.28	49.72	24.58	34.61
TiO_2	wt%	0.43	0.41	0.83	0.41	0.09	0.63	0.38	0.51	0.74	2.42	2.24	0.11	0.12	0.13	0.19	0.18	0.20
Al_2O_3	wt%	13.37	13.56	16.19	9.27	1.66	15.97	6.58	9.32	12.07	17.45	14.13	2.91	0.29	3.47	8.55	9.08	6.49
Fe_2O_3	wt%	3.37	4.99	11.93	30.53	74.50	15.48	35.05	13.58	20.15	19.84	14.24	74.62	68.07	48.20	25.61	54.86	43.84
MnO	wt%	0.08	0.04	0.14	0.02	0.01	0.03	0.02	1.30	0.53	0.08	0.29	0.01	0.02	0.02	0.24	0.02	0.28
MgO	wt%	0.83	0.45	4.00	0.57	0.11	0.73	0.25	8.22	5.18	14.84	4.92	0.10	0.08	0.17	0.21	0.19	0.40
CaO	wt%	0.85	0.24	1.37	0.47	1.48	0.58	0.78	10.14	5.03	0.32	6.32	0.32	0.40	4.76	1.82	0.42	2.05
Na_2O	wt%	3.40	0.22	0.23	0.12	0.06	0.26	0.09	0.18	0.17	2.20	2.53	0.09	0.10	0.04	0.13	0.33	0.12
K_2O	wt%	5.53	7.01	4.61	3.01	0.44	5.04	2.04	2.83	3.71	0.47	0.93	0.47	0.03	1.36	4.01	1.64	1.78
P_2O_5	wt%	0.07	0.08	0.28	0.21	0.16	0.20	0.25	0.28	0.32	0.24	0.20	0.56	0.29	0.17	0.28	0.85	0.55
CO_2	wt%	0.27	0.20	1.47	0.21	0.08	0.08	0.26	16.12	7.62	0.04	1.57	0.13	0.21	0.33	2.44	0.26	2.52
S	wt%	0.05	0.05	0.20	1.06	1.04	0.08	0.44	0.04	0.15	0.02	0.03	0.82	1.04	2.36	1.78	2.61	2.15
Cu	ppm	38	120	1304	2365	865	420	4561	425	300	100	203	725	195	15227	10891	34082	17403
U_3O_8	ppm	13	22	25	90	47	90	115	32	37	24	2	102	70	266	396	490	675
Au	ppm	0.001	0.006	0.04	0.31	0.16	0.04	0.61	0.10	0.04	0.31	0.01	0.25	0.05	0.87	0.33	0.43	0.58
Ag	ppm	0.33	0.1	0.4	1.0	<1	<1	1.3	<1	<1	<1	<1	0.9	<1	2.8	1.0	4.7	4.4
As	ppm	4.9	10.2	59	553	440	49	177	45	101	198	5.8	317	274	351	82	49	61
Ba	ppm	0.09	0.1	0.3	3.54	3.97	0.27	0.86	0.12	0.66	0.03	233.75	3.4	4.22	3.84	0.69	0.3	0.2
La	ppm	0.010	0.011	0.015	0.09	0.09	0.07	0.11	0.02	0.02	0.01	<0.025	0.15	0.16	0.26	0.14	0.17	0.15
Ce	ppm	0.019	0.021	0.023	0.12	0.11	0.10	0.16	0.04	0.04	0.03	<0.05	0.22	0.23	0.33	0.21	0.26	0.24
Co	ppm	4.3	11	39	12	3.1	16	13	82	97	357	44	24	4.1	45	65	231	112
Cr	ppm	<20	<20	570	<20	35	322	28	2296	2731	n.d.	85	<20	<20	<20	<20	<20	47
Mo	ppm	0.9	2.0	10.6	117	212	6.6	79	6.4	13	3	4.3	110	131	422	68	32.9	38.6
Ni	ppm	2.8	3.0	184	17	7.8	42	6.8	382	315	73	52	4.8	2.6	2	7	22	13
Pb	ppm	14	14	24	93	76	44	59	37	41	5	14	46	53	58	475	78	75
Sr	ppm	91	49	99	n.d.	616	213	n.d.	n.d.	n.d.	n.d.	163	648	n.d.	447	407	2480	386
V	ppm	15	14	147	<10	51	127	19	167	175	<10	336	25	28	10	14	54	29
Zn	ppm	41	137	239	91	25	188	110	1437	769	425	270	58	26	36	10911	74	116
Zr	ppm	338	349	237	258	40	250	314	129	183	144	147	102	50	123	190	129	154

All analyses conducted at AMDEL-Bureau Veritas, Adelaide

Abbreviations: Alt dike = altered mafic dike, Bx-cp = chalcopyrite-bearing hematite-rich breccias, Bx-Mo = hematite-rich breccias from the deep zone of mineralization, and Bx-mt = magnetite+hematite breccias, Bx-Zn = sphalerite-bearing granite-rich breccias, Dol = plagioclase-pyroxene-phyric dolerite dikes, HEMQ = hematite+quartz+barite breccias, KASH = chlorite-bearing, laminated sandstone and mudstone, KFMU = polymictic volcanic conglomerate, KHEMQ = well bedded, hematite-rich sandstone, mudstone and conglomerate-breccia, RDG = Roxby Downs Granite, RDG-ser alt = weakly altered RDG, VASH = thinly laminated, very hematite-rich mudstones, VBx = hematite-rich breccias consisting of porphyritic felsic volcanic clasts

[1] Samples from the 10,000 sample MLA data set

relict orthoclase, albite, and quartz (volcanic and granitoid derived); some beds contain detrital chromite. This facies may be locally reddish-brown and hematite-altered. Additional diagnostic properties include Al (9 wt %), Mg (2.5%), K (3.5–4.5%), Ti (0.45–0.55%), and elevated concentrations of Cr (400–500 ppm), V (100–200 ppm), Ni (100–300 ppm), and Zn (200–400 ppm).

The well-bedded, hematite-rich sandstone, mudstone, and conglomerate-breccia facies association consists of hematite clasts, granite clasts, granitoid- and volcanic-derived quartz and feldspar fragments, and felsic volcanic clasts, but lacks mafic igneous components. This association contains anomalous concentrations of Mo (~150 ppm) and As (>200 ppm), which are likely due to a hydrothermal overprint.

Some intervals within the hematite-rich sandstone, mudstone, and conglomerate facies association include delicately laminated, hematite-rich mudstone. Successive laminae consist of red, gray, and black hematite, which resemble banded iron formation.

Polymictic volcanic conglomerate-breccia is a minor component of the bedded clastic facies, consisting of well-rounded felsic and mafic volcanic clasts. It occurs interbedded with the green sandstone and hematite-rich sandstone facies, and is distinguished by being much coarser grained (most clasts are 1–6 cm). The beds are thick and internally massive, and are poorly sorted and vary from clast- to matrix-supported. The felsic and mafic volcanic clasts are texturally and compositionally identical to felsic and mafic lavas in the Gawler Range Volcanics.

Ultramafic volcanic units: Remnants of intensely altered chromite-bearing, olivine-phyric picrite occur immediately below the unconformity, vary between 15 to 40 m thick in eight drill holes (Fig. 2A), and may represent a single or multiple units. The picrite is in contact with various hematite-rich breccias (see below); the contact is intensely altered and sheared. The picrite is strongly carbonate-hematite altered but retains a well-preserved porphyritic texture comprising evenly distributed, skeletal, relic olivine phenocrysts (~1 mm diam) and carbonate-hematite-filled amygdales (up to ~1 cm). There are carbonate-hematite veins 1 to 5 mm in width. Additional diagnostic properties of picrites include elevated concentrations of Cr (>1,000 ppm), V (100–200 ppm), and Ni (300–500 ppm). The location and texture suggest that this picrite was a lava.

(Pre- to) Synbrecciation rock units

Mafic and felsic igneous intrusions are present mainly as dikes. Four types of dikes are distinguished by composition and alteration: (1) aphanitic, sericite-hematite–altered probably mafic dikes, (2) sericite-altered, olivine-phyric mafic dikes, (3) sericite ± chlorite ± hematite-altered, plagioclase-pyroxene-phyric mafic dikes, and (4) one quartz-phyric felsic dike. The mafic dikes are steeply dipping and intrude Roxby Downs Granite, bedded clastic facies, and Olympic Dam Breccia Complex breccias; some are mineralized and contemporaneous with breccia formation and mineralization. Multiple generations of dikes commonly intrude along the same structures.

Aphanitic, sericite-hematite-altered dikes consist of microcrystalline sericite and chlorite, and may be replaced by hematite. Crystals (~100 μm) of zircon, rutile, xenotime, bastnasite, and florencite are also present and are probably of hydrothermal origin. Even though original textures are not preserved, slightly elevated concentrations of titanium and magnesium suggest an original mafic composition. The dikes vary in thickness from < 0.5 m up to >40 m and have inferred strike lengths of up to 1 km. The contacts with granite-rich breccias (see below) are sharp at depth and become more gradational with decreasing depth. These dikes are best exposed in the deeper parts of the northwestern ore zones.

Olivine-phyric basaltic dikes are generally strongly sericite-altered but retain a relic porphyritic texture comprising pseudomorphs of olivine phenocrysts in very fine groundmass. Olivine appears to have been the only phenocryst and the high abundance of olivine suggests these dikes may have been ultramafic in composition. The dikes are a few centimeters to decimeters across and have sharp contacts with the granite and more irregular, lobate or brecciated contacts with the hematite-rich breccia. The contacts are marked by ~3-mm-wide, formerly glassy zones in the dike and ~5-mm-wide oxidized zones in the granite.

Plagioclase-pyroxene-phyric basaltic dikes consist of plagioclase and pyroxene and range from relatively fresh to strongly chlorite ± sericite ± hematite altered. The phenocrysts are generally fine (1–2 mm) and hard to distinguish from the groundmass in the strongly altered samples. These dikes may appear as cross-cutting, green chlorite-rich intervals, and contain disseminated pyrite and chalcopyrite and veins of chalcopyrite, pyrite with fluorite, and barite. They are generally steeply dipping and relatively narrow (1–5 m across) although much wider (tens of m) intervals can occur. These dikes have similar composition and texture to the Gairdner Dykes.

One intensely altered, quartz-phyric dike has been intersected in the deepest vertical drill hole (RD2773) in the southeastern part of the Olympic Dam Breccia Complex at a depth of ~1,900 to 2,300 m. The dike has intruded weakly brecciated, chlorite-altered Roxby Downs Granite and is steeply dipping and brecciated along its margins. The dike is composed of melt inclusion-bearing quartz phenocrysts in a groundmass of quartz and sericite with minor zircon and apatite, implying an original rhyolitic composition.

Olympic Dam Breccia Complex

The principal components of the Olympic Dam Breccia Complex are derived from Roxby Downs Granite, with lesser contributions from Gawler Range Volcanics, bedded clastic facies, and hydrothermal sources (Reeve et al., 1990, provided detailed textural descriptions of the breccias). Alteration and brecciation intensity increase from the edges of the Olympic Dam Breccia Complex toward the deposit center. Breccia composition and textural characteristics are gradational; thus, most rocks within the Olympic Dam Breccia Complex form a continuum, ranging from sericite-altered Roxby Downs Granite to sericite-altered, granite-rich breccias through to hematite-rich breccias in the deposit center.

Subdivision of breccias of the Olympic Dam Breccia Complex, based on identifying primary rocks, is complicated because of intense hydrothermal alteration. However, at the deposit scale, compositional changes across the breccia continuum are systematic. Photographs of unaltered Roxby Downs Granite through to hematite-rich breccias are shown in Figure 3A,

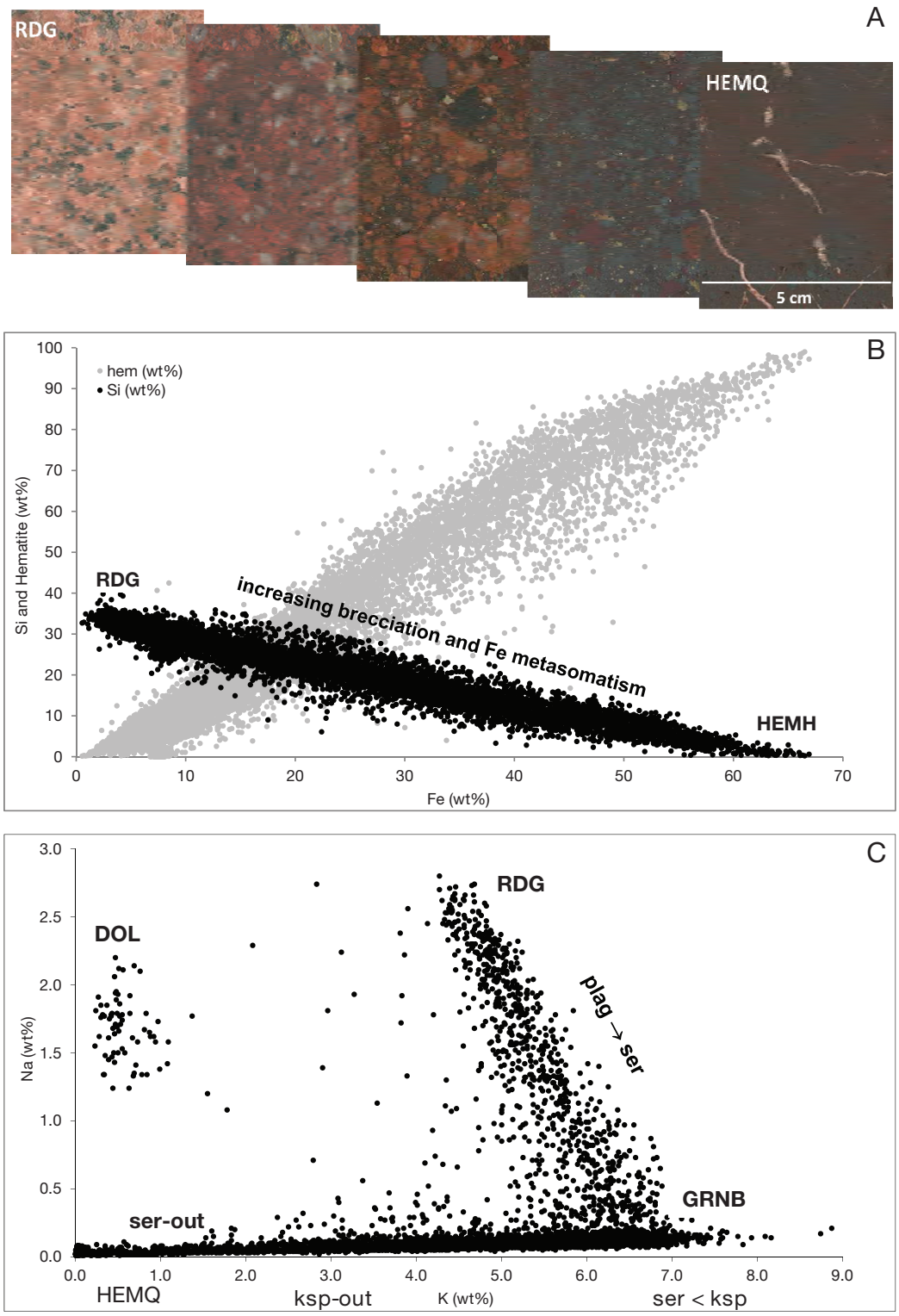


FIG. 3. Progressive alteration and brecciation of the Roxby Downs Granite (RDG). A. Drill core images of unaltered Roxby Downs Granite through to HEMQ (hematite+quartz+barite) breccias (left to right). The width of each rock slab is 5 cm. B. Relationship between whole-rock iron, silicon, and hematite concentration. C. Whole rock K vs. Na scatterplot. Note the two major trends; plagioclase alteration to sericite (spatially occurs outside of the 5 wt % Fe envelope and prior to significant brecciation of the Roxby Downs Granite), and K-feldspar alteration to sericite, followed by sericite alteration to hematite. Abbrevations are: Gairdner dikes (DOL), progressive sericite alteration of plagioclase (plag → ser), sericite altered, weakly brecciated Roxby Downs Granite (GRNB), sericite wt % < orthoclase wt % (ser < ksp), orthoclase replaced by sericite and hematite (ksp-out), sericite replacement by hematite (ser-out), and hematite-rich breccias with minor granite-derived components (HEMH). The data in the scatter plots are from the 10,000-sample MLA data set.

arranged in order of increasing hematite concentration. A scatterplot (Fig. 3B) of Fe (whole-rock Fe content) versus hematite wt % (MLA modal mineralogy) and Fe versus Si whole-rock composition shows the gradation from unaltered Roxby Downs Granite to hematite-rich breccias. Based on these Fe versus hematite and Si relationships, granite-derived breccias are subdivided (for logging and mapping purposes) according to their hematite content.

Post-brecciation rock units

Gairdner Dykes: The weakly altered dikes vary from coarse, equigranular dolerite to finely porphyritic basalt. Equigranular pyroxene and plagioclase crystals are intergrown in the dolerite or form phenocrysts in the porphyritic basalt; magnetite is also present and causes a characteristic magnetic property (magnetic susceptibility ~>100 × 10^{-3} SI units). Multiple generations of dikes are present in some cases, early dolerite being intruded by later porphyritic basalt. Contacts of these dikes with the Roxby Downs Granite or Olympic Dam breccias are sharp and marked by perlite or palagonite-altered glassy margins typically a few millimeters across. The dolerite can be weakly chlorite altered and incipient hematite alteration may also be present in the shallower examples. Narrow carbonate veins are common. Although weakly altered, this dolerite is not mineralized and is magnetic. Additional diagnostic properties are Cr, V, Ni, and Ti concentrations of 50 to 100 ppm, 300 ppm, 50 to 100 ppm, and 1.5 to 2 wt %, respectively.

Neoproterozoic to Cambrian sedimentary rocks: Approximately ~320 m of flat-lying, shallow marine shale, quartzite, and dolomite overlie the eroded upper surface (sub-horizontal unconformity) of the Roxby Downs Granite and Olympic Dam Breccia Complex.

Structure

Several published and unpublished structural studies at Olympic Dam have been based on underground mapping data (Sugden and Cross, 1991; T.J. Sugden, pers. commun., 1992; Widdup et al., 2004; C. McCuaig, pers. commun., 2005), oriented drill core measurements and acoustic televiewer logging (G. Dishaw, pers. commun., 2009), and regional geophysical datasets (N. Hayward, pers. commun., 2007; Hayward and Skirrow, 2010). The structural interpretation completed by G. Dishaw (pers. commun., 2009) is summarized below, based on the analyses of ~40,000 structures from underground geological mapping, ~21,000 structures from oriented drill core measurements, and ~69,000 structures from acoustic televiewer logging.

A complex array of brittle faults cut the deposit (Fig. 4). In addition to numerous local-scale structures, five main fault sets are recognized. The N-S, NW, WNW, and NE faults were all steeply dipping and in place pre- and/or synmineralization.

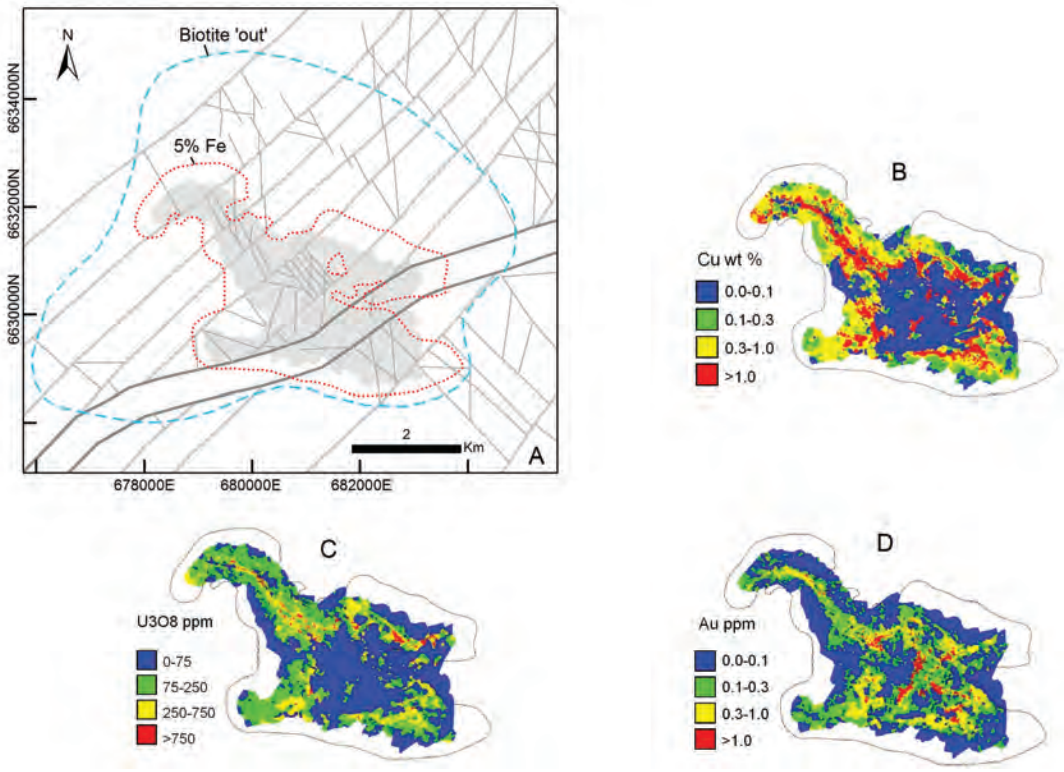


FIG. 4. A. Simplified structural map of the Olympic Dam Breccia Complex. Limits of unaltered Roxby Downs Granite lie outside the blue dashed line, and >5 wt % Fe is inside the red stippled line. The inner gray shape represents the outline of the 2011 resource model. Five major sets of faults are shown: N-S, NW, WNW, NE, and Masher's. Fault timing in relation to mineralization is described in the text. Structures from oriented drill core measurements, acoustic televiewer logging, and underground geological mapping were used to identify the faults (G. Dishaw, pers. commun., 2009). B-D. Simplified maps showing the distribution of (B) Cu, (C) U_3O_8, and (D) Au at the –350 mRL based on the 2011 resource model. Note the strong spatial linear distribution of high grades and correlation between Cu, U_3O_8, and Au. There is also a strong correlation with Fe concentration (Fig. 7).

N-S faults: These faults are generally discontinuous and offset by NW, NE, and WNW sets; the longest examples extend over 1 km. Hematite and copper enrichments are associated with this strike and form basin-like junctions with WNW faults, where bedded clastic facies and pre- to synmineralization dikes are located; there is minor evidence of late reactivation.

NW faults: NW faults are regionally continuous (e.g., Elizabeth Creek fault zone; Hayward and Skirrow, 2010) and offset by NE faults and Masher's fault. These faults are associated with hematite alteration, copper mineralization, pre- to synmineralization mafic dikes and late (postmineralization event) dolerite intrusions and form basin-like junctions with earlier N-S faults; there is some evidence of late reactivation.

WNW faults: The WNW faults are regionally discontinuous and appear to be splays of NW faults in the vicinity of NE faults, or slightly earlier than the NW faults. They are associated with hematite alteration and copper mineralization where these faults exist in the immediate hanging wall of NE faults; they can also be associated with molybdenum enrichment. There is minor reactivation, intensified close to Masher's fault with sinistral offsets.

NE faults: NE faults are regionally continuous (e.g., Todd Dam fault zone; Hayward and Skirrow, 2010) and offset NW, WNW, and NS fault sets. There is an association with hematite alteration and copper mineralization where these faults intersect WNW faults. They are mapped regionally as being reverse faults but at deposit scale, the evidence suggests normal movement. They are locally strongly reactivated by Masher's fault, with sinistral movement, and were reactivated as late as the Cambrian as deformation zones in the Andamooka Limestone.

Masher's fault: ENE faults appear to have been active over a long period since the Neoproterozic and represent a major regional aeromagnetic feature (~100 km long). Masher's fault is the local name used at Olympic Dam for the Jubilee fault zone (Hayward and Skirrow, 2010). Masher's fault does not control or offset either the distribution of hematite breccias or copper mineralization.

Hydrothermal Alteration

The principal hydrothermal alteration minerals are hematite, magnetite, sericite (i.e., fine-grained muscovite, illite, phengite and paragonite), quartz, chlorite, siderite, fluorite, and barite. Table 3 lists all Olympic Dam minerals. Iron oxide addition and sericite alteration of igneous feldspars are the two dominant alteration effects within the Olympic Dam Breccia Complex and are common to all alteration assemblages. Three major hematite alteration transitions (Fig. 2A) are alteration of igneous biotite ("biotite-out"), granite-rich breccias (~5 wt % Fe; whole-rock Fe content), and hematite-rich breccias (~20 wt % Fe; whole-rock Fe content). Four alteration assemblages contain variable combinations of at least two of the dominant hydrothermal alteration minerals.

The spatial distributions of the hydrothermal alteration minerals are complex in detail and very difficult to quantify based on visual logging estimates alone. Scatter plots of whole rock Fe vs Si composition (Fig. 3B) and K versus Na composition (Fig. 3C) show clear correlations that reflect mineralogical changes. These plots demonstrate that broad deposit-wide alteration patterns are present. Modal mineralogy of the major rock-forming minerals in the Roxby Downs Granite and Olympic Dam Breccia Complex (Table 4), plotted as a function of the whole-rock Fe concentration (Fig. 5), displays the relationship between the primary and hydrothermal minerals.

Hematite alteration

Hematite forms pseudomorphs of preexisting igneous orthoclase and hydrothermal minerals such as magnetite, siderite, chlorite, sericite, and rarely sulfides; hematite is also precipitated in vugs and veins.

Alteration of igneous biotite: The transition from unaltered to weakly altered Roxby Downs Granite to the outer margins of the Olympic Dam Breccia Complex is gradational and is defined by chlorite alteration of igneous biotite (i.e., "biotite-out" contour; Figs. 1, 2, 6A) and hematite alteration of igneous magnetite. Incipient sericite alteration of plagioclase occurs outside of the "biotite-out" boundary, whereas biotite does not exist inside the boundary.

Granite-rich breccias: The presence of hematite as matrix, clasts, or veins (i.e., inside the "5% Fe" contour; Figs. 1, 2, 6A) is used to establish the limits of hematite alteration. The granite-rich breccias have a broad distribution and exhibit a wide range of textures that reflect their variable intensities and styles of brecciation. These breccias are generally fractured and veined granites, with angular clasts of brecciated granite, and hematite and other hydrothermal components; volcanic components are rare. The texture of the granite is progressively destroyed with the increase in matrix constituents.

Hematite-rich breccias: At approximately 20 wt % Fe (e.g., "20% Fe" contour; Figs. 1, 2, 6A), hematite becomes the most abundant component in the breccia; this marks the transition from granite-rich to hematite-rich breccias. The hematite-rich breccias are also derived from Roxby Downs Granite, but reflect a more intense degree of brecciation and a higher proportion of hydrothermal constituents relative to the granite-rich clasts. Hematite-rich breccias are the major host rocks for sulfide mineralization. Breccia styles are variable; clasts tend to be angular and equidimensional (generally less than 20 cm diam), and clasts from preexisting breccias are common. Breccias generally become more matrix supported with increasing hematite content, and the matrix itself is usually red-brown to black hematite. Hematite breccias can be heterolithic, dominated by hematite and granite clasts, but with volcanic and bedded clastic facies clasts and single minerals (particularly siderite, chalcopyrite, barite, and fluorite) locally present as clasts. The distribution of hematite breccias is more discrete and confined to narrower zones than those of granite breccias; the hematite breccias are interpreted to have been the main hydrothermal fluid pathways related to the formation of the deposit. In plan view (Figs. 2A, 6A), the hematite-rich breccia zones have a broad distribution across the deposit; locally single hematite-rich breccias are elongated in a NW-SE direction and are steeply dipping. The long axis of the NW trend roughly coincides with the PD1 photo lineament and is subparallel to the G9C gravity lineament of O'Driscoll (1985), strongly suggesting that intersecting major regional- and continental-scale structure(s) may have focussed breccia development and hydrothermal activity.

TABLE 3. Olympic Dam Mineralogy

Mineral	Formula	Qualitative Abundance[1]
Ore minerals		
Pyrite	FeS_2	Minor
Chalcopyrite	$CuFeS_2$	Minor
Bornite	Cu_5FeS_4	Minor
Chalcocite	Cu_2S	Minor
Digenite	Cu_9S_5	Minor
Djurelite	$Cu_{31}S_{16}$	Minor
Idaite	Cu_3FeS_4	Sparse
Covellite	CuS	Sparse
Roxbyite	$Cu_{1.78}S$	Sparse
Carrollite	$CuCo_2S_4$	Trace
Cobaltite	(Co,Fe)AsS	Trace
Saffl orite	$(Co,Fe)(As,S)_2$	Sparse
Lollingite	$(Fe,Co,Ni)As_2$	Sparse
Enargite	Cu_3AsS_4	Sparse
Domeykite	$(Cu,Fe)_3As$	Sparse
Arsenopyrite	FeAsS	Sparse
Tennantite-tetrahedrite	$(Cu,Ag,Zn,Fe)_{12}(As,Sb)_4S_{13}$	Trace
Molybdenite	MoS_2	Trace
Sphalerite	(Zn,Fe)S	Trace
Galena	PbS	Trace
Stibnite	Sb_2S_3	Sparse
Pyrrhotite	$Fe_{1-x}S$	Sparse
Electrum	$(Au,Ag,Cu,Fe)^o$	Sparse
Native copper	Cu^o	Sparse
Native silver	Ag^o	Sparse
Native arsenic	As^o	Sparse
Native tellurium	Te^o	Sparse
Native bismuth	Bi^o	Sparse
?	Au-Pd	Sparse
Calaverite	$AuTe_2$	Sparse
Petzite	Ag_3AuTe_2	Sparse
Hessite	Ag_2Te	Sparse
Acanthite	Ag_2S	Sparse
Allargentum	Ag_4Sb	Sparse
Silver-Hg	(Ag,Hg)	Sparse
Volynskite	$AgBiTe_2$	Sparse
Bismoclite	(Bi,Fe)OCl	Sparse
Kawazulite	$Bi_2(Te,S)_3$	Sparse
Wittichenite	Cu_3BiS_3	Sparse
Clausthalite	PbSe	Sparse
Altaite	PbTe	Sparse
Coloradoite	HgTe	Sparse
Tellurobismuthite	Bi_2Te_3	Sparse
Bismuthinite	Bi_2S_3	Sparse
Melonite (?)	$NiTe_2$	Sparse
Cuprite	Cu_2O	Sparse
Tenorite	CuO	Sparse
Scheelite	$CaWO_4$	Sparse
Wolframite	$(Fe,Mn)WO_4$	Sparse
Cassiterite	SnO_2	Sparse
Uranium and REE minerals		
Uraninite-pitchblende	$(U,Pb,Ca,Fe,Cu,Ce,Nd,Y)O_2$	Trace
Coffinite	$(U,P,Y,Ca,Ce,Nd,Fe)(SiO4)_{1-x}(OH)_{4x}$	Trace
Brannerite	$(U,Ca,Ce)(Ti,Fe)_2O_6$	Trace
Zircon	$(Zr,U,Th,Ca)SiO_4$	Trace
Thorite	$(Th,U,Fe,Y,P,Ca,Pb)SiO_4$	Trace
Thorianite	$(Th,U)O_2$	Trace
Uranothorite	$(U,Th,Y,P,Fe,Ca,Nd)SiO_4$	Trace
Bastnasite	$(Ce,La,Nd,Pr,Ca)(CO_3)F$	Trace
Florencite	$(Ce,La,Nd,Ca,Sr)(Al,Fe)_3(PO_4)_2(OH)_6$	Trace
Monazite	$(Ce,La,Nd,Fe,Ca)PO_4$	Trace
Synchysite	$Ca(REE,Y,Fe,Th,U)(CO_3)_2F$	Trace
Britholite	$(Ce,Ca)_5(SiO_4,PO_4)_3(OH,F)$	Trace
Xenotime	$(Y,Yb)PO_4$	Trace
Crandallite group	$(Ce,La,Nd,Ca,Sr)(Al,Fe)_3(SO_4PO_4)_2(OH)_6$	Trace
Gangue minerals		
Hematite	Fe_2O_3	Major
Magnetite	Fe_3O_4	Minor
Chromium spinel	$(Fe,Mg,Ca)(Cr,Al,Ti)_2O_4$	Trace[2]
Manganosite	(Mn,Fe,Ca)O	Sparse
Quartz	SiO_2	Major
Chlorite group	$(Fe,Mg)_5Al(Si_3Al)O_{10}(OH,O)_8$	Major
Biotite	$K_2(Mg,Fe)_6(AlSi_3O_{10})_2(OH,Cl,F)_4$	Major[3]
Muscovite (sericite)	$(K,Na)(Fe,Mg,Al)_2(Si_3Al)O_{10}(OH,F,Cl)_2$	Major
Amphibole	$(Na,K)(Ca,Na,Mn)_2(Fe,Mg,Al,Ti)_5(Si,Al)_8O_{22}(O,Cl)$	Major[3]
Orthoclase-microcline	$(K,Na)AlSi_3O_8$	Major
Plagioclase	$(Na,Ca,Fe)(Si,Al)_3O_8$	Major[3]
Albite	$NaAlSi_3O_8$	Major
Schorl	$NaFe^{+2}{}_3Al_6(BO_3)_3Si_6O_{18}(OH)_4$	Trace
Corundum	$(Al,Fe)_2O_3$	Sparse
Diaspore	AlO(OH)	Sparse
Zunyite	$Al_{13}Si_5O_{20}(OH,F)_{18}Cl$	Sparse
Kaolinite	$Al_2Si_2O_5(OH)_4$	Sparse
Siderite	$(Fe,Mn,Mg,Ca)CO_3$	Major-minor
Ankerite	$Ca(Fe,Mg,Mn)(CO_3)_2$	Minor
Dolomite	$Ca(Mg,Fe,Mn)(CO_3)_2$	Minor
Calcite	$(Ca,Mn,Fe)CO_3$	Minor
Fluorite	CaF_2	Major-minor
Sellaite	MgF_2	Trace
Barite	$(Ba,Sr)SO_4$	Major-minor
Celestite	$SrSO_4$	Trace
Anhydrite	$CaSO_4$	Trace
Fluorapatite	$Ca(PO_4)_3F$	Trace
Rutile	TiO_2	Trace
Ilmenite	$(Fe^{2+},Mn)TiO_3$	Sparse
Ilmenorutile	$(Ti,Nb,Fe^{3+})_3O_8$	Sparse
Sphene	$CaTiSiO_5$	Trace[3]

Minerals identified via optical microscopy, scanning electron microscopy, or XRD

[1] Relative abundances: major > minor >trace > sparse

[2] Mineral found in the minor rock units (bedded clastic facies rocks and mafic-ultramafic dikes)

[3] Igneous mineral in the Roxby Downs Granite

Sericite alteration

Sericite is widespread throughout the Olympic Dam Breccia Complex where it occurs as an alteration product of igneous sodic plagioclase (albite and oligoclase), igneous orthoclase, and hydrothermal chlorite; sericite is replaced by hematite in hematite-quartz-barite breccias. Incipient sericite alteration of sodic plagioclase is present in relatively unaltered Roxby Downs Granite (RDG-ser category in Fig. 5). Complete sericite replacement of plagioclase occurs in samples with Fe concentration up to 5 wt %. The concentration of orthoclase steadily

TABLE 4. Modal Mineralogy of the 10,000-Sample MLA Data Set

Mineral	Abundance (wt %)
Pyrite	0.4614
Chalcopyrite	0.9261
Bornite	0.3346
Chalcocite	0.1388
Covellite	0.0068
Carrollite	0.0004
Cobaltite	0.0012
Safflorite	0.0001
Lollingite	0.0003
Domeykite	0.0001
Tennantite	0.0072
Molybdenite	0.0015
Sphalerite	0.0115
Galena	0.0012
Pyrrhotite	0.0090
Native Copper	0.0001
Clausthalite	0.0002
Altaite	0.0000
Tellurobismuthite	0.0000
Bismuthinite	0.0003
Uraninite	0.0049
Coffinite	0.0159
Brannerite	0.0119
Zircon	0.0549
Thorite	0.0023
Uranothorite	0.0028
Bastnasite	0.0833
Florencite	0.0660
Monazite	0.0184
Synchysite	0.0124
Xenotime	0.0045
Crandallite	0.1097
Fe oxide	30.5338
Quartz	30.8395
Chlorite group	1.3240
Sericite	18.1930
Orthoclase	9.8422
Albite	0.6371
Schorl	0.0521
Corundum	0.0001
Diaspore	0.0001
Zunyite	0.0042
Kaolinite	0.0060
Siderite	2.6574
Siderite_Mn	0.2432
Ankerite	0.1849
Dolomite	0.1327
Fluorite	1.1795
Sellaite	0.0002
Barite	1.2252
Anhydrite	0.0108
Apatite	0.1029
Rutile	0.2411
Ilmenite	0.0447
Ilmenorutile	0.0001
Unclassified	0.0857

decreases as the Fe concentration increases and essentially disappears (<1 wt %) where Fe >35 wt %. There is no evidence for the presence of hydrothermal orthoclase. Figure 6 shows the location of four potassium aluminosilicate alteration zones (ksp > ser, ser > ksp, ser only, hematite-quartz-barite breccias).

Quartz alteration

Hydrothermal quartz is likely due to precipitation of silica that was released via sericite alteration of the igneous feldspars. The quartz occurs in 1- to 5-mm-wide microveinlets with apatite, magnetite, and/or siderite in the significantly altered, unbrecciated granite and as anhedral to subhedral crystals in the breccias. In addition, hydrothermal quartz occurs as 20- to 50-m-thick quartz veins in altered Roxby Downs Granite, located in the extreme southeastern part of the Olympic Dam Breccia Complex. The strike length of these veins exceeds 800 m, and the zone is approximately 200 m wide. However, the quartz veins are not geochemically anomalous in any trace metals. Timing of the quartz veins is difficult to establish because no crosscutting relationships with the Gairdner Dykes or the unconformity at the top of the basement have been exposed via drilling or underground development. Silicification also occurs as irregular zones along the edges the hematite-quartz-barite breccias.

Chlorite alteration

Mg-Fe-chlorite replaced igneous biotite and amphibole in weakly altered Roxby Downs Granite and replaced mafic-ultramafic clasts in hematite-breccias. Chlorite alteration intensity increases near contacts with mafic and ultramafic dikes and intrusions, but commonly grades into intensely sericite altered breccias away from the contacts with pre- to synbrecciation dikes. In the granite-derived breccias, chlorite tends to be more abundant at depth, Fe-rich, and typically forms pseudomorphs of feldspars. Sericite typically overprints chlorite.

Alteration of minor rock types

Contacts of bedded clastic facies with hematite-rich breccias are faults or appear to be gradational, but the intense alteration makes interpretation difficult. Mapping the lateral extent of the bedded clastic facies is complicated by the presence of texturally destructive hematite alteration; this alteration includes sericite and chlorite alteration in the bedded clastic facies that is replaced by hematite. Clasts of feldsparphyric felsic lavas in hematite breccias are variably altered to sericite and hematite.

Alteration assemblages within altered granite, and granite- and hematite-rich breccias

Reduced Fe oxide assemblage (magnetite+apatite+siderite+chlorite+quartz): Reduced Fe oxide alteration occurs as microveinlets in altered, unbrecciated Roxby Downs Granite and as isolated zones in deep, paragenetically early hematite-rich breccias (Fig. 6C). The minerals form euhedral to anhedral grains, with magnetite and siderite being partially to completely replaced by hematite; very rare textures suggest partial magnetite alteration of hematite, and siderite also occurs as fragments of veins. Sulfides typically consist of pyrite with lesser amounts of chalcopyrite; bornite and chalcocite are typically not present.

Oxidized Fe oxide assemblage (hematite+sericite+fluorite): Reduced Fe oxide alteration is replaced by oxidized Fe oxide alteration in the deeper parts of the deposit. Hematite is more abundant than magnetite and its concentration increases towards the deposit center (Fig. 6A). This alteration assemblage is strongly associated with sulfide minerals, including chalcopyrite, bornite, and chalcocite with minor amounts of pyrite. Based on optical microscope examination of polished sections of drill core, a significant, but difficult to

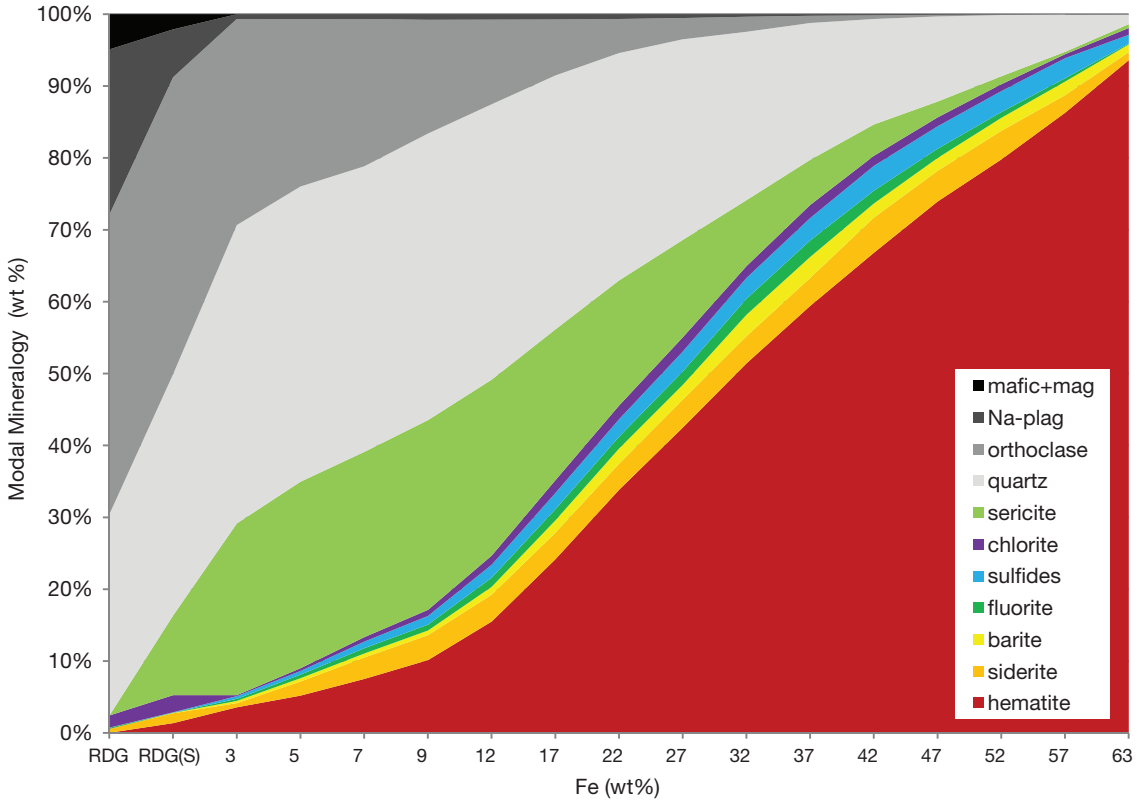


FIG. 5. Percentages (wt %) of the major igneous and hydrothermal minerals for different whole-rock Fe concentrations. The igneous minerals are sodic-plagioclase (Na-plag), orthoclase, biotite+amphibole+magnetite (~1% magnetite: mafic + mag). The hydrothermal minerals are hematite, siderite, barite, fluorite, sulfides, chlorite, and sericite. The average mineral abundances for the entire 10,000-sample MLA data set are shown here. The concentration of quartz increases as plagioclase is altered to sericite. This is likely due to re-precipitation of some of the silica released from plagioclase alteration. The zonation of siderite-fluorite-barite described in the text is not apparent here because the data are not filtered for spatial context. Hydrothermal magnetite is included in the hematite field because quantification of magnetite concentration is only semiquantitative at present. Based on magnetic susceptibility measurements of drill core, the magnetite content varies from <0.1 to ~20 wt %.

quantify, proportion of the hematite at depth has replaced Fe^{+2} minerals (magnetite, siderite, and chlorite). Rare magnetite inclusions (~1–5 μm diam) occur in hematite grains at shallower depths which is suggestive of the presence of a lesser amount of magnetite in the upper levels of the Olympic Dam Breccia Complex. The reduced and oxidized Fe oxide assemblages are located within the "5% Fe" contour (Fig. 6).

Hematite-quartz-barite assemblage (hematite+quartz+barite): The alteration assemblage hematite-quartz-barite (HEMQ, Fig. 6A) is defined by a lack of aluminosilicate and sulfide minerals. Hematite and quartz occur as clasts within a matrix of hematite and quartz grains; intersecting sets of narrow (<1 mm) barite veins are also present. Sulfide mineralization is confined to minor late-stage veins and joints, with sulfide mineral concentrations rarely greater than 0.05 wt %. This alteration assemblage has margins that are commonly silicified and barite veined, and may contain gold-only mineralization. A variety of textures is observed that probably reflect different, extremely altered, protoliths (e.g., granite, felsic and mafic volcanic fragments, and bedded clastic facies). Hematite-quartz-barite can be hard and silicified or soft and highly porous. Relic granite or felsic volcanic clast textures can be preserved, or the breccia can simply consist of fine-grained hematite. Hematite-quartz-barite breccias typify the deposit center, yet other volumetrically smaller zones occur along the dominant NW-SE axis of alteration and mineralization.

Intense sericitic alteration assemblage (sericite+quartz+Al-OH). This alteration assemblage occurs mainly at shallow depths ENE of the central hematite-quartz-barite breccias zone (Fig. 6A). Granite-rich breccias are bleached (> 35 wt % sericite and 5–10 wt % Fe), have < 0.3 wt % Cu, but may contain ~> 0.3 ppm Au. Relict orthoclase is present along with ~ 1.5 wt % hydrothermal (?) albite, with rare occurrences of zunyite, kaolinite, and diaspore. Strongly altered mafic-ultramafic dikes and intrusions are commonly closely associated with this alteration. This alteration style also occurs as isolated zones (alteration remnants) in hematite-altered breccias in the northwestern extension of the deposit. Similar textures with more intense hematite alteration also occur near the edges of the hematite-quartz-barite breccias (Fig. 6A). The presence of sericite with zunyite, kaolinite, or diaspore is typical of advanced argillic alteration usually attributed to interaction with a relatively acidic fluid during some period of alteration (Hemley et al., 1980).

Mineralization

The vast majority of Cu, U_3O_8, and Au mineralization is associated with hematite-rich breccias (Fe > 20 wt %). Significant

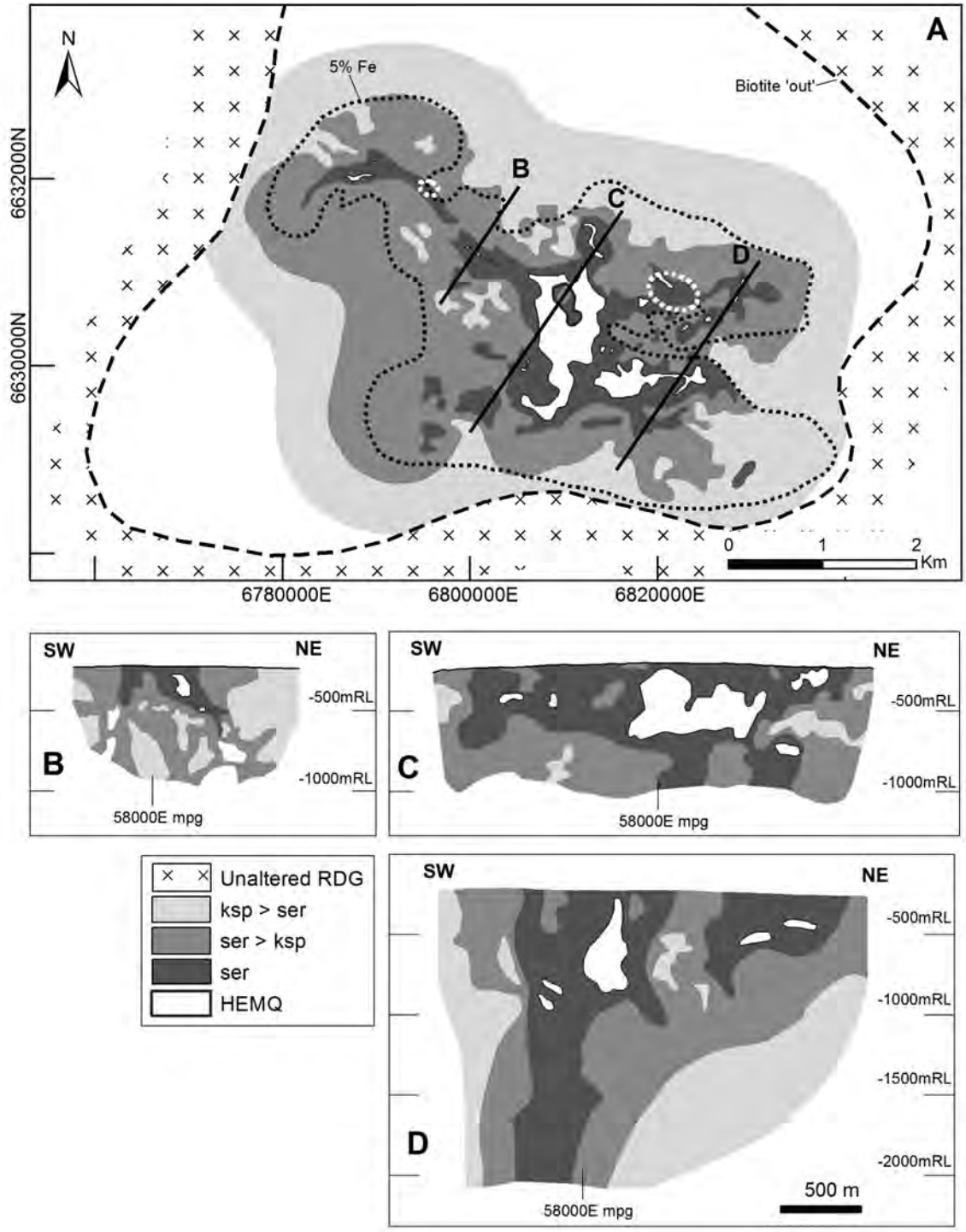


FIG. 6. Simplified potassium aluminosilicate hydrothermal alteration map at the –350 mRL (A) and cross sections (B-D) of the Olympic Dam Breccia Complex showing the progressive change in potassium aluminosilicate mineral abundances. Abbreviations: orthoclase wt % > sericite wt % (ksp > ser), sericite wt % > orthoclase wt % (ser > ksp), sericite with <1 wt % orthoclase (ser only), and <1 wt % sericite (HEMQ = hematite-quartz-barite breccias). Compare with Figure 2. The stippled areas show the locations of intense sericitic alteration (possibly advanced argillic alteration).

mineralization also occurs within granite-rich breccias (Fe 5–20 wt %), and minor mineralization occurs within the other pre-brecciation rock units. Strong evidence for structural control is the linear distribution of high-grade Cu (>1 wt %) at –350 mRL (Fig 4B). Plans of high-grade Au and U_3O_8 also show similar linear distribution patterns (Fig. 4C-D). Multiple generations of mafic to ultramafic dikes have also intruded along preexisting zones of weakness (e.g., fractures and faults). The evidence for the spatial association between mafic dikes and breccias zones is becoming increasingly clear

as the deeper and more peripheral parts of the deposit in the northwestern extension are exposed by closer spaced diamond drilling.

At depth in the northwest, massive and very fine grained, quartz-absent hematite veins are present in altered to weakly altered Roxby Downs Granite. The transition from hematite vein to altered granite and poorly developed granite breccia occurs sharply. As depth decreases, the veins become flanked by hematite-rich breccia. At even shallower depths, the Fe-rich breccia grades into heterolithic breccia which then grades into granite-rich breccia. The evidence for the controls on veins is obliterated by brecciation and intense alteration. Remnants of variably hematite-altered mafic to ultramafic dikes occur in the strongly hematite-altered veins; the remnants become more abundant with increasing depth. The very fine hematite grain size indicates that the hematite probably replaced a preexisting lithology that also contained no quartz. Copper mineralization is variable, but typically concentrated along the vein and dike contacts; sulfides were precipitated in the matrix of breccias as the abundance of the matrix increased.

There is a positive correlation between increasing Cu, U_3O_8, and Au (Fig. 7A) and increasing Fe up to 40–45 wt %; above which the concentrations of Cu, U_3O_8, and Au decrease. However, not all Fe-rich samples have Cu, U_3O_8, and Au mineralization (Fig. 7B), which demonstrates that not all hematite-rich breccias are mineralized.

Copper, uranium, gold, and silver are the only metals recovered from the existing operation; however, the deposit also contains anomalous concentrations of F, S, C, As, Ba, Bi, Cd, Co, Cr, Fe, In, Mo, Nb, Ni, P, Pb, Se, Sn, Sr, Te, V, W, Y, Zn and rare earth elements (REE; in particular light REE; LREE). Detailed descriptions of the ore textures are provided by Roberts and Hudson (1983), Oreskes and Einaudi (1990, 1992), and Reeve et al. (1990).

Copper

The primary sulfide minerals are pyrite, chalcopyrite, bornite, and chalcocite/djurleite/digenite (hereafter referred to as chalcocite) with relative deposit-scale abundances of 25, 50, 18, 7%, respectively (Table 4). Copper mineralization occurs dominantly as disseminated sulfide mineral grains ranging in size from <20 μm up to several millimeters, with the average size of ~100 μm. The sulfides display a simple zonation at the scale of 1-m drill core intervals up to the deposit scale. Tennanite-tetrahedrite and enargite are present at relatively low abundances and appear to be located in the ores associated with the deep mineralized zone (i.e., the area above and surrounding mineralization occurring below –950mRL; Figs. 2D, 6D). Covellite, native copper, and tenorite/cuprite are very rare. Most of the sulfides do not display textures indicative of formation under supergene conditions (i.e., chalcocite replacing chalcopyrite or pyrite), suggesting that they most likely precipitated under hypogene conditions. However, when covellite is present it occurs along the edges and in cracks in bornite located near the basement unconformity, suggesting that if supergene enrichment did occur, it has been removed by erosion. Native copper and tenorite/cuprite are locally associated with chalcocite, but usually not associated with the basement unconformity.

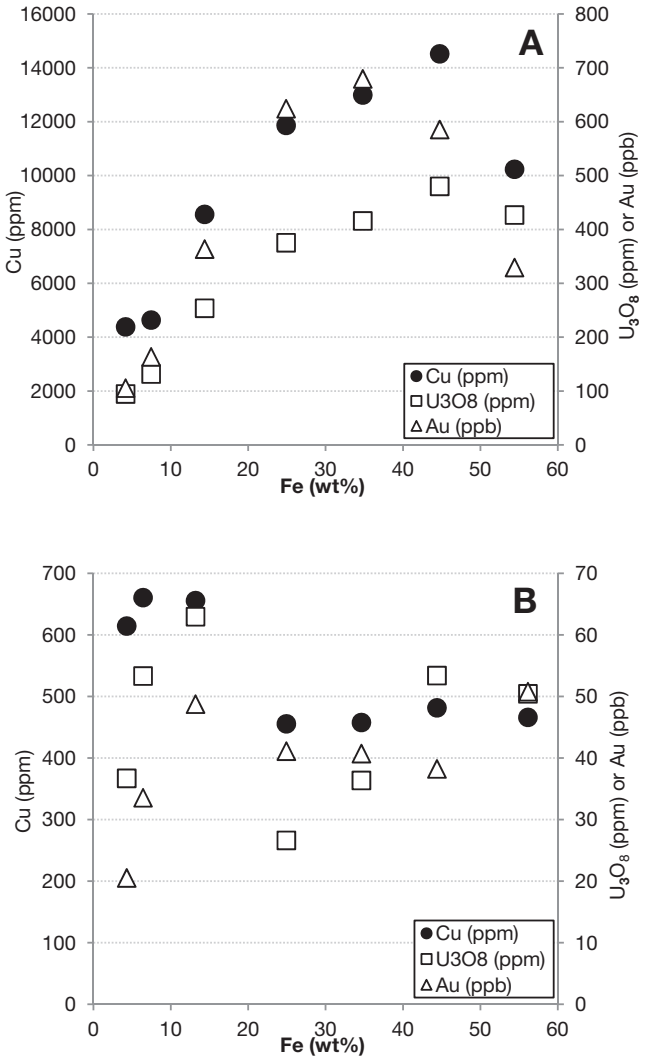


FIG. 7. Conditional means Cu, U_3O_8 and Au vs. Fe concentration for samples with (A) Cu ≥1,000 ppm and (B) Cu <1,000 ppm. A. There is a strong positive correlation of Cu, U_3O_8, and Au with Fe up to ~40–45 wt % Fe, above which the concentrations of Cu, U_3O_8, and Au decrease. B. No strong correlation exists between Cu, U_3O_8, and Au with Fe in samples with <1,000 ppm Cu. The data are from the 10,000-sample MLA data set.

Sulfide veins are not common in the hematite breccias, but do occur in the granites and granite breccias located on the deposit edge. Massive sulfide mineralization is extremely rare.

Photomicrographs illustrating typical sulfide textures and gangue mineral associations are shown in Figure 8. Pyrite, chalcopyrite, bornite, and chalcocite can be intergrown with the major gangue minerals (hematite, quartz, sericite, orthoclase, chlorite, barite, fluorite, and siderite). Bornite and chalcocite are rarely associated with siderite.

Two generations of pyrite are present: (1) coarse-grained euhedral crystals (Fig. 8A) commonly associated with magnetite, with or without chalcopyrite, where the chalcopyrite is not replacing the pyrite, and (2) more commonly as anhedral to subrounded grains that are partially replaced by chalcopyrite (Fig 8B). Pyrite replacement of chalcopyrite has not been observed. Very rare textures of small pyrite grains in massive bornite are present.

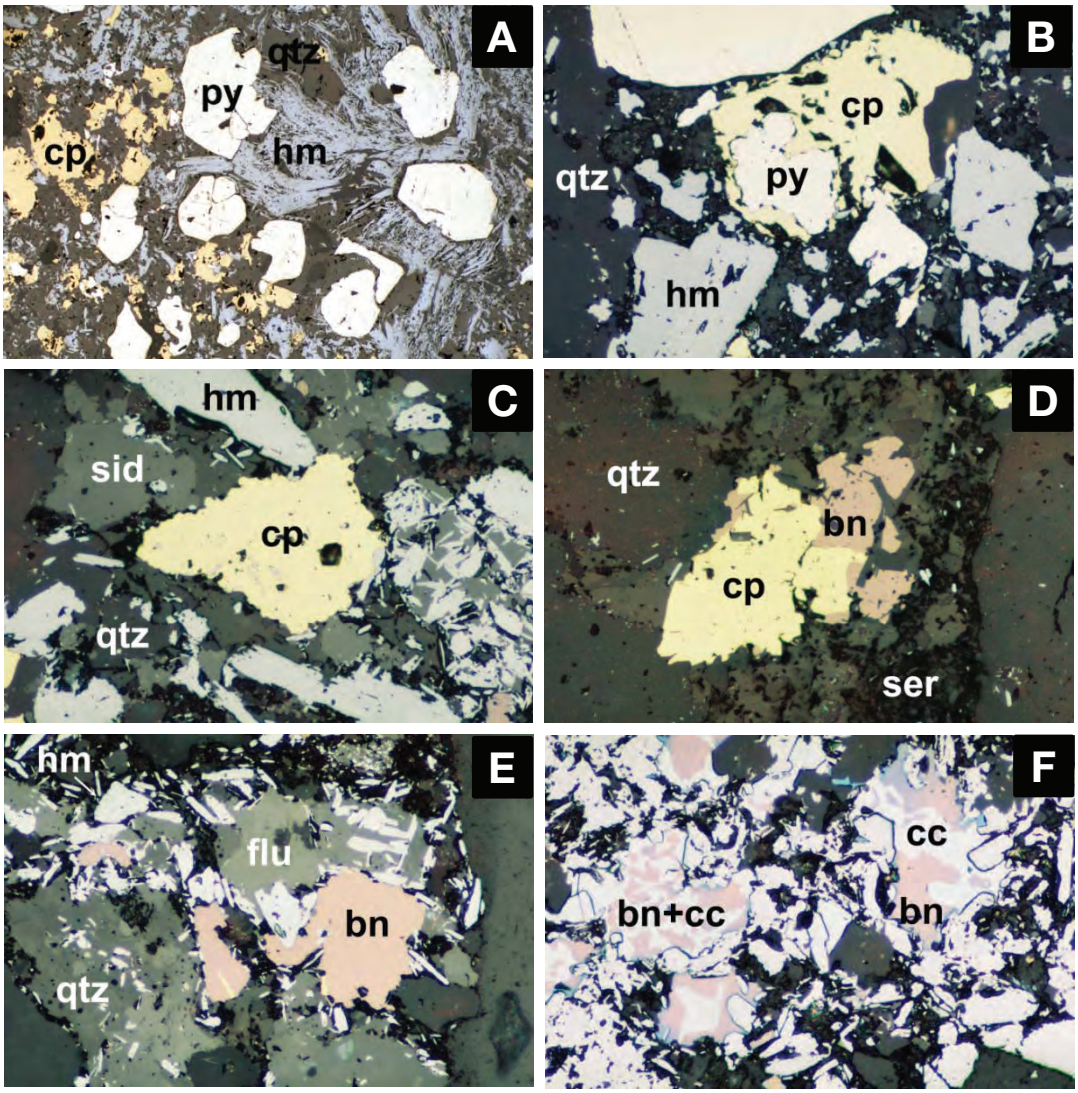


FIG. 8. Photomicrographs showing typical sulfide mineral textures. A. Early euhedral pyrite (py) and hematite (hm) with later chalcopyrite (cp). B. Chalcopyrite replacement of pyrite, with quartz (qtz), and hematite. C. Chalcopyrite with siderite (sid), quartz, and hematite. D. Co-precipitation of chalcopyrite and bornite (bn) in a matrix of sericite (ser) and quartz. E. Bornite with fluorite (flu), quartz, and hematite. F. Bornite-chalcocite (bn+cc) exsolution texture. Field of view for each image = 330 μm.

Chalcopyrite can also occur as (1) isolated grains (Fig. 8C), (2) coprecipitated with bornite (Fig. 8D), (3) as grains being replaced by bornite, or (4) rarely, replacing bornite. Chalcopyrite-bornite pairs are not as common as chalcopyrite-pyrite or bornite-chalcocite pairs. Bornite can occur as (1) isolated grains (Fig. 8E), (2) grains being replaced by chalcocite, or (3) most commonly as myrmekitic bornite-chalcocite intergrowths (Fig. 8F). Chalcocite occurs as isolated grains and rarely replaces bornite.

Uranium

More than 90% of the uranium in the deposit is present in uraninite-pitchblende (hereafter referred to as uraninite), coffinite, and brannerite. Uranium also occurs as a minor to trace concentrations in hematite, thorite-uranothorite, thorianite, thorite, crandallite, xenotime, zircon, REE-group minerals (i.e., florencite, bastnasite, monazite, synchysite), pyrite, chalcopyrite, bornite, and chalcocite. The average grain size for uraninite, coffinite, brannerite, thorite, and thorianite is ~20 μm, with a range from <0.5 μm to >1 mm. The uranium minerals are usually disseminated throughout all sulfides and gangue minerals, but also occur as microveinlets at relatively high U_3O_8 concentrations. Uraninite-coffinite and coffinite-brannerite are commonly complexly intergrown (Fig. 9). Remobilization of uranium occurred on the micron to meter scale, and was most common at scales of ~<0.5 mm.

Logging the uranium mineral species during routine drill core logging is not possible because of the relatively low abundances and very fine grain sizes. Our understanding of the deposit-wide uranium mineral speciation and distribution is largely based on the 10,000-sample MLA modal mineralogy dataset. The relative abundances of uraninite, coffinite, and brannerite change with increasing Fe concentration, with an increase in uraninite (Fig. 10). The deposit-wide average

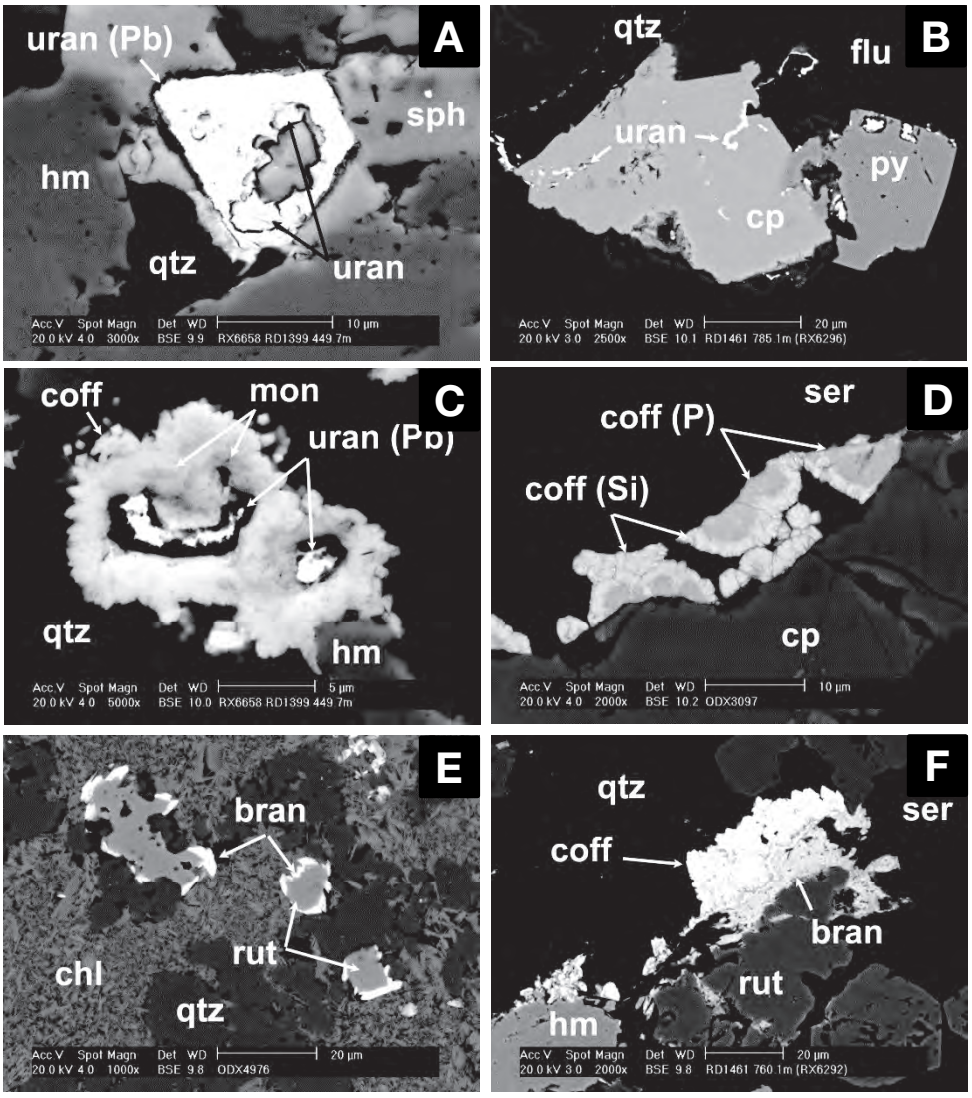


FIG. 9. Backscattter electron images showing typical uraninite/pitchblende-coffinite-brannerite textures. A. Two generations of uraninite (early Pb-rich and late Pb-poor); B. uraninite with chalcopyrite, pyrite, and quartz; C. coffinite replacing high-Pb uraninite; D. chemically zoned coffinite (Si- and P-rich); E. brannerite precipitation on rutile; F. coffinite replacing brannerite. Abbreviations are: Pb-rich uraninite (uran (Pb)), uraninite (uran), Si-rich coffinite (coff (Si)), P-rich coffinite (coff (P)), coffinite (coff), brannerite (bran), hematite (hm), quartz (qtz), sphalerite (sph), chalcopyrite (cp), pyrite (py), fluorite (flu), monazite (mon), rutile (rut), chlorite (chl), and sericite (ser).

relative proportions of brannerite, coffinite and uraninite are 31, 56, 13%, respectively, but the latter increases to >40% at high Fe concentrations.

Gold

Electrum (with a variable Au-Ag-Cu-Fe composition) is the dominant gold-bearing phase, but gold also occurs as calaverite, petzite, and tetra-auricupride. Gold in the deposit has three general mineralogical and rock type associations: (1) as inclusions in or attached to sulfide minerals, (2) as inclusions in sericite and/or quartz in intensely sericitized granite breccias, and (3) as inclusions in quartz, hematite, and barite along the margins of hematite-quartz-barite breccias. Gold particles are typically ~1 to 20 μm in diameter; however, rare large nuggets and bonanza veins occur in hematite-rich gold-only zones. The composition of electrum particles forms two distinct populations: (1) >95% Au with <5% Ag + Cu where associated with the sulfides, and (2) <90% Au with ~10% Ag + Cu + Fe where associated with sericite, quartz, hematite, or barite.

Silver

Silver occurs in electrum, petzite, acanthite, allargentum, rarely as native silver but predominantly as hessite inclusions in sulfide minerals, particularly bornite. It can also occur as a trace element in bornite, chalcocite, and tennantite-tetrahedrite. Hessite grain size is typically <10 μm.

Rare earth elements

Olympic Dam ore contains ~0.17 wt % La and 0.25 wt % Ce. The major REE minerals are bastnasite and florencite, with lesser abundances of synchysite, monazite, xenotime, zircon,

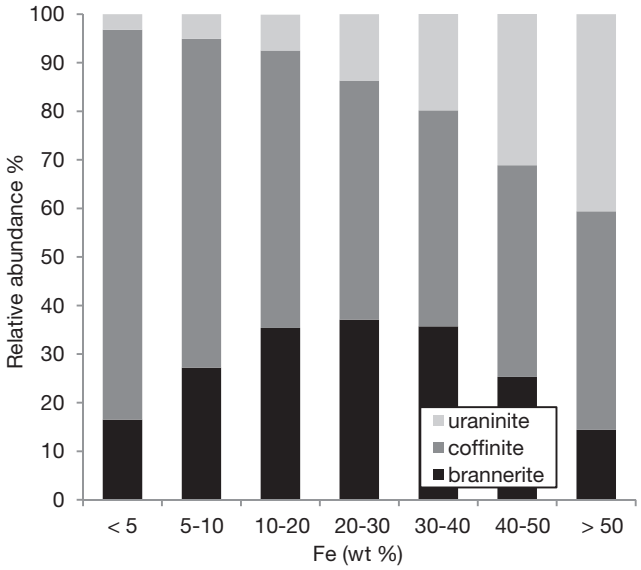


FIG. 10. Conditional means uranium mineral relative % for uraninite, coffinite, and brannerite vs. Fe concentration. Coffinite is the dominant uranium mineral with lesser proportions of uraninite and brannerite. However, the relative abundance of uraninite increases with increasing whole-rock Fe wt %. The data are from the 10,000-sample MLA dataset.

and crandallite. The REE also occur in minor to trace concentration in uranium minerals; like the uranium minerals, the REE minerals occur as disseminated grains in gangue and sulfide minerals, with an average grain size of 35 μm. Although Olympic Dam ores contain anomalous concentrations of REE, the concentrations are not sufficiently high to justify extraction at present.

Carbon, fluorine, and sulfur

The carbonate minerals are siderite, ankerite, dolomite-calcite, bastnasite, and synchysite; no other carbon-bearing minerals have been identified. The relative abundances of carbonates are 87.5, 5.6, 4, 2.5, and 0.4%, respectively (Table 4). Siderite is iron rich but displays extensive substitution of iron by manganese, magnesium, and calcium [(Fe,Mg,Mn, Ca)CO_3]. Ankerite and calcite are typically associated with mafic-ultramafic dikes.

Fluorite is the predominant fluorine-bearing mineral. Sericite, chlorite, apatite, bastnasite, and synchysite also contains fluorine.

In addition to the sulfides, sulfur also occurs in barite and anhydrite. The relative abundances of barite and anhydrite are 99.2 and 0.8 wt %, respectively.

Siderite, fluorite, and barite occur as veins and as clasts and matrix components of breccias; there is no evidence for siderite, fluorite, or barite replacement of preexisting primary or hydrothermal minerals.

Other elements (Zn, Pb, As, Mo, Sn, W, Bi, Sb, Se, Te, Co, Ni)

Sphalerite is the main Zn-bearing mineral, and typically occurs intergrown with chalcopyrite and to a lesser extent with bornite or pyrite. Sphalerite grain sizes and gangue mineral associations are similar to the other sulfides (i.e., chalcocite, bornite, chalcopyrite and pyrite) and its composition is Zn rich and Fe poor. In most ore zones, the concentration of Zn rarely exceeds 0.03 wt %; however, Zn occurs up to 0.5 to 1 wt % in the northwest, and up to 1 to 2 wt % in the southeastern extremities of the deposit.

The concentration of Pb across all ore types is usually <100 ppm, largely in galena, clausthalite, and altaite; radiogenic Pb occurs in all uranium-bearing minerals. Coarse-grained (up to a few millimeters, usually ~100 μm) galena is usually associated with sphalerite but can also occur in microveinlets cutting hematite-quartz-barite breccias; however, most galena, clausthalite, and altaite grains are <10 μm in diameter.

Cobaltite, tennantite-tetrahedrite, and As-bearing pyrite are the major mineralogical hosts of As; other As minerals include enargite, safflorite, domeykite, lollingite, arsenopyrite, and native arsenic (As^o). The average concentration of As in ore is ~200 ppm, but varies significantly across the deposit, reaching concentrations of up to a few thousand ppm in Au-only ores, and up to 4,500 ppm in ores with anomalous concentrations of Mo.

The average Mo concentration in ore is <60 ppm. However, the hematite-quartz-barite breccias are enriched in Mo up to 100 to 200 ppm, 100 to 1,000 ppm in and surrounding the deep zone of mineralization to the southeast, and 100 to 1,000 ppm in magnetite-bearing breccias and rare, narrow quartz-molybdenite veinlets on the deposit edges. Molybdenite is the only Mo mineral that has been identified and occurs as 5 to 20 μm spherical aggregates of curved plates and as 100 μm plates in quartz veins; it is commonly associated with sulfides and quartz, but may occur with any of the uranium and gangue minerals.

The average concentrations of W and Sn in ore are ~100 and ~30 ppm, respectively. Both W and Sn concentrations are elevated where Mo is high, but the converse is not true. Tungsten concentrations reach maximum values of ~2,000 ppm (about twice that of Mo), and occurs as scheelite and wolframite. Scheelite grain size varies from <20 μm to >100 μm, and occurs mainly with gangue and sulfide minerals, and wolframite occurs as <10 μm-sized inclusions in scheelite. Cassiterite is the only Sn-bearing mineral identified, with grain sizes <5 μm, usually as inclusions in hematite.

Selenium occurs as clausthalite whereas tellurium is contained in several minerals; altaite, tellurobismuthite, hessite, petzite, volynskite, coloradoite, calaverite, kawazulite, and native tellurium. Tellurobismuthite, bismuthite, bismoclite, wittichenite, and native bismuth (Bi^o) are the main Bi hosts; selenium, tellurium, and bismuth minerals typically occur as <10-μm-sized inclusions in the sulfides. The average concentrations of Se, Te, and Bi in ore are 5, 2.5, and 7 ppm, respectively.

Tennantite-tetrahedrite and stibnite are the only observed Sb-bearing minerals, which has an average concentration of ~12 ppm across all ore types.

Cobalt is most typically associated with chalcopyrite-pyrite. The average Co concentration in ore is ~80 ppm, but can reach maximum values of ~900 ppm, principally hosted in cobaltite, carrollite, and cobaltiferous pyrite. Minor concentrations of Co can also be present in chlorite, safflorite, and lollingite. The grain size of cobaltite varies from <5 μm up to >100 μm. Cobaltite and carrollite commonly occur along the boundary between pyrite-chalcopyrite intergrowths.

Background concentrations of Ni within the ore deposit are typically <10 ppm. Concentrations greater than 10 ppm are reliable indicators of the presence of intense sericite- or hematite-altered mafic to ultramafic volcanic rocks, which are usually not mineralized. Pyrite can contain up to 1,000 ppm Ni, so is probably the main Ni-bearing mineral, with lesser amounts of lollingite.

Mineralogical Zonation

Intense Fe oxide and sericite alteration along with repeated brecciation of the Roxby Downs Granite and other minor rock units have resulted in texturally complex breccias which are difficult to interpret at the macroscopic scale. However, when the fundamental components (minerals and elements) of the breccias are examined, mineralogical and geochemical trends are apparent (Figs. 3B, C, 5). Although over 90 minerals (Table 3) have been identified at Olympic Dam, 15 minerals (hematite, quartz, sericite, orthoclase, chlorite, siderite, fluorite, barite, pyrite, chalcopyrite, bornite, chalcocite, sphalerite, galena, and molybdenite) allow 98.4% of the mineralogical variability within the Olympic Dam Breccia Complex to be described (Table 4). Spider diagrams illustrate geochemical trends, which help to define patterns in mineralogical and trace element zonation.

Geochemical trends

Roxby Downs Granite-normalized diagrams show the effects of increasing Fe oxide alteration on granite-derived elements (Fig. 11) and elements introduced by the hydrothermal system (Fig. 12), including REE (Fig. 13) at different Cu concentration ranges; data come from the 10,000-sample MLA dataset. Various ranges of Cu concentration are used to determine the differences between Cu-unmineralized (<300 ppm Cu; Figs. 11A, 12A, 13A), weakly mineralized (300–1,000 ppm Cu; Figs. 11B, 12B, 13B), moderately mineralized (1,000–3,000 ppm Cu; Figs. 11C, 12C, 13C) and mineralized (≥3,000 ppm Cu; Figs. 11D, 12D, 13D) breccias; Au-only samples (very low sulfides) have been removed from this analysis. Within each Cu category, conditional means were calculated for each element at increasing Fe concentrations (<5, 5–10, 10–20, 20–30, 30–40, 40–50, ≥50 wt % Fe; App. Tables A1-A4).

Granite-derived elements (Fig. 11): With increasing Fe oxide alteration, Al, Be, Ca, Hf, K, Li, Mg, Mn, Na, Rb, Si, Th, Ti, and Zr are depleted (relative to Roxby Downs Granite) for all Cu concentration categories. The degree of depletion for the elements increases with increasing Fe concentration. Initial sericite alteration of sodic plagioclase depleted Na, whereas Ca and Mn were initially depleted (chlorite alteration of amphibole and biotite) but became enriched via the precipitation of fluorite and Mn-bearing siderite in moderately mineralized and mineralized Cu categories (i.e., in samples containing ≥1000 ppm Cu).

Hydrothermal elements: The hydrothermal elements (excluding REEs; Fig. 12) were introduced (normalized to Roxby Downs Granite) with increasing Fe oxide alteration, including Ag, As, Au, Ba, Bi, Cd, Cl, Co, CO_2, Cr, Cu, F, Fe, In, Mo, Nb, Ni, P, Pb, S, Sb, Sc, Se, Sn, Sr, Ta, Te, U, V, W, Y, and Zn. A group of elements (Mo, Sb, W, As, S, Te, Ba, and Sn) were enriched in the Cu-unmineralized and weakly mineralized Cu category samples prior to (or distal to) significant addition of Cu plus U and F and may represent the geochemical signatures of proximal versus distal mineralization or paragenetically earlier mineralization. The hydrothermal elements are all enriched, and all increase up to ~45 wt % Fe, then the enrichment patterns change.

REE (Fig. 13): Olympic Dam is enriched in LREE. The LREE are enriched whereas the medium and heavy REE (MREE, HREE) are depleted in Cu-unmineralized, weakly mineralized, and moderately mineralized Cu category samples (<3,000 ppm Cu; Fig. 13A-C). The MREE and HREE also become enriched in the mineralized category (Cu ≥3,000 ppm; Fig. 13D). The REE pattern for samples with >50% Fe and ≥3,000 ppm Cu shows depletion of the REE relative to samples with <50% Fe.

Cu-Fe sulfide mineral zonation

Roberts and Hudson (1983) and Reeve et al. (1990) reported zonation of pyrite, chalcopyrite, bornite and chalcocite based on geological logging and mapping observations. Reeve et al. (1990) reported a margin-to-center gross deposit zonation as follows:

pyrite → chalcopyrite → bornite → chalcocite → (native copper) → Au^o

The boundary from chalcopyrite to bornite (referred to as the bn-cp interface) is a well-defined and readily mapped feature across the deposit. The interface marked the transition from sulfur-rich species (pyrite and chalcopyrite) at depth and near the deposit periphery to sulfur-poor species (bornite and chalcocite) shallower and toward the central regions of the deposit. A map displaying the depth to the bn-cp interface was produced along with a schematic deposit-scale cross section showing the bn-cp interface as a relatively continuous feature. Two additional cross sections based on drill core logging showed the interface as a locally, highly convoluted surface (Reeve et al., 1990; their figs. 2B, 5, 7, 9). The absolute and relative proportions of pyrite, chalcopyrite, bornite, and chalcocite have not been discussed in previously published accounts of the sulfide mineralogy at Olympic Dam.

At the 1-m scale, the quantitative abundances of pyrite, chalcopyrite, bornite, and chalcocite can be calculated from whole rock Cu, S and Ba assays based on four assumptions that have been validated by geological logging, polished section observations, and modal mineralogy (i.e., the 10,000-sample MLA dataset). The assumptions are as follows: (1) copper occurs predominantly in chalcopyrite, bornite, and chalcocite; (2) sulfur occurs in sulfide (pyrite, chalcopyrite, bornite, and chalcocite), and sulfate (barite) minerals; (3) barium occurs as barite; and (4) the sulfide species occur individually or as distinct binary pairs (pyrite, chalcopyrite-pyrite, chalcopyrite, chalcopyrite-bornite, bornite, bornite-chalcocite, chalcocite) over the scale of 1 m (the standard assay interval length).

Quantitative modal mineralogy measurements on the 10,000-sample MLA dataset shows that ~98% of the sulfides are pyrite, chalcopyrite, bornite, and chalcocite (Table 4) and > 99% of the copper occurs as chalcopyrite, bornite, and chalcocite. Even though sulfur occurs in barite and anhydrite in addition to the sulfides, barite accounts for >99% of the sulfate-bearing minerals present with the sulfide minerals; Ba

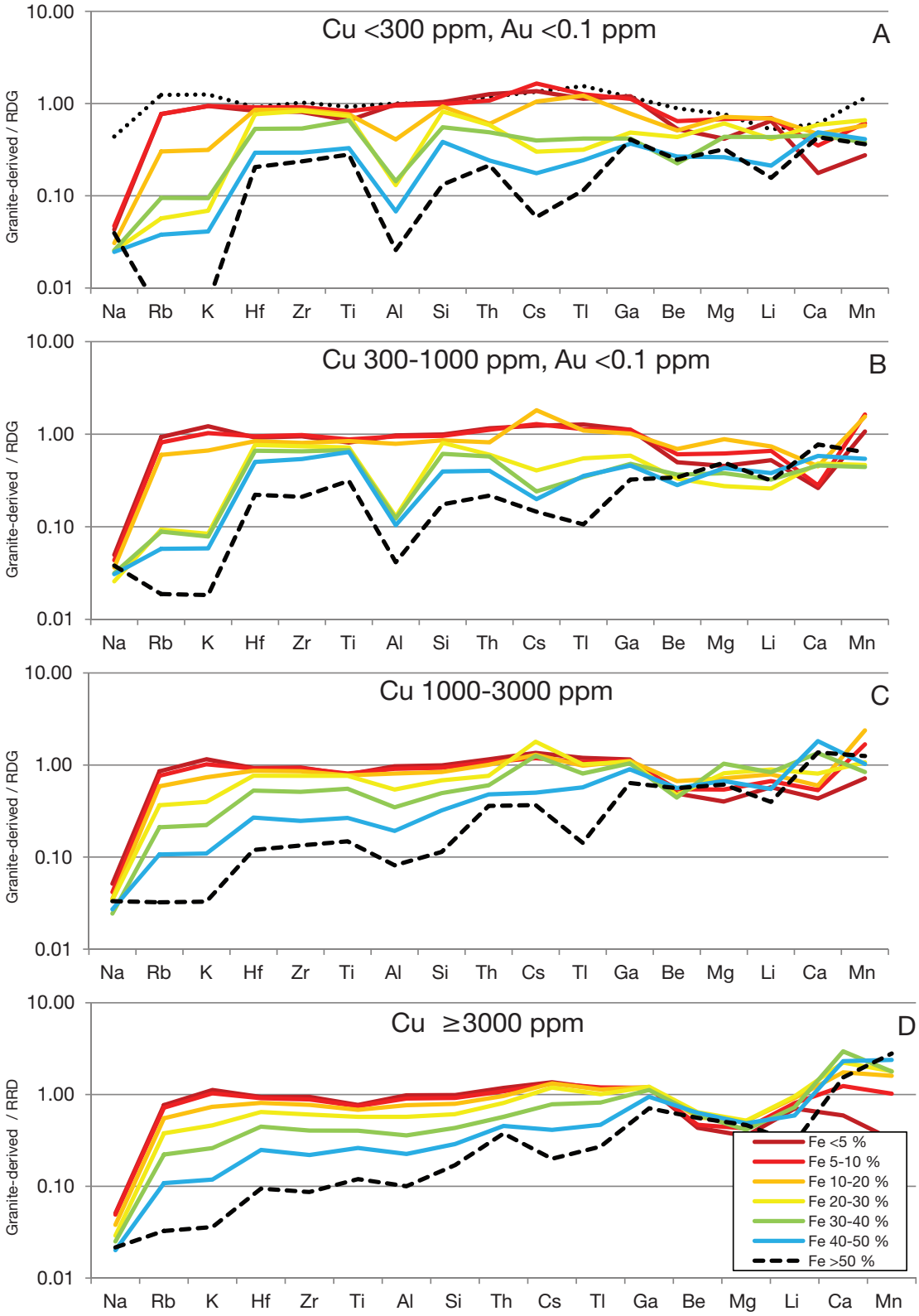


FIG. 11. Roxby Downs Granite-derived (Al, Be, Ca, Hf, K, Li, Mg, Mn, Na, Rb, Si, Th, Ti, Zr) element mobility for (A) Cu-unmineralized (<300 ppm Cu and <0.1 ppm Au), (B) weakly mineralized (300–1,000 ppm Cu and <0.1 ppm Au), (C) moderately mineralized (1,000–3,000 ppm Cu), and (D) mineralized (≥3,000 ppm Cu) samples. Within each Cu category, conditional means were calculated for each element at increasing Fe concentrations (< 5, 5–10, 10–20, 20–30, 30–40, 40–50, ≥50 wt %. The graphs show the conditional means normalized to the Roxby Downs Granite. The data are from the 10,000-sample MLA dataset.

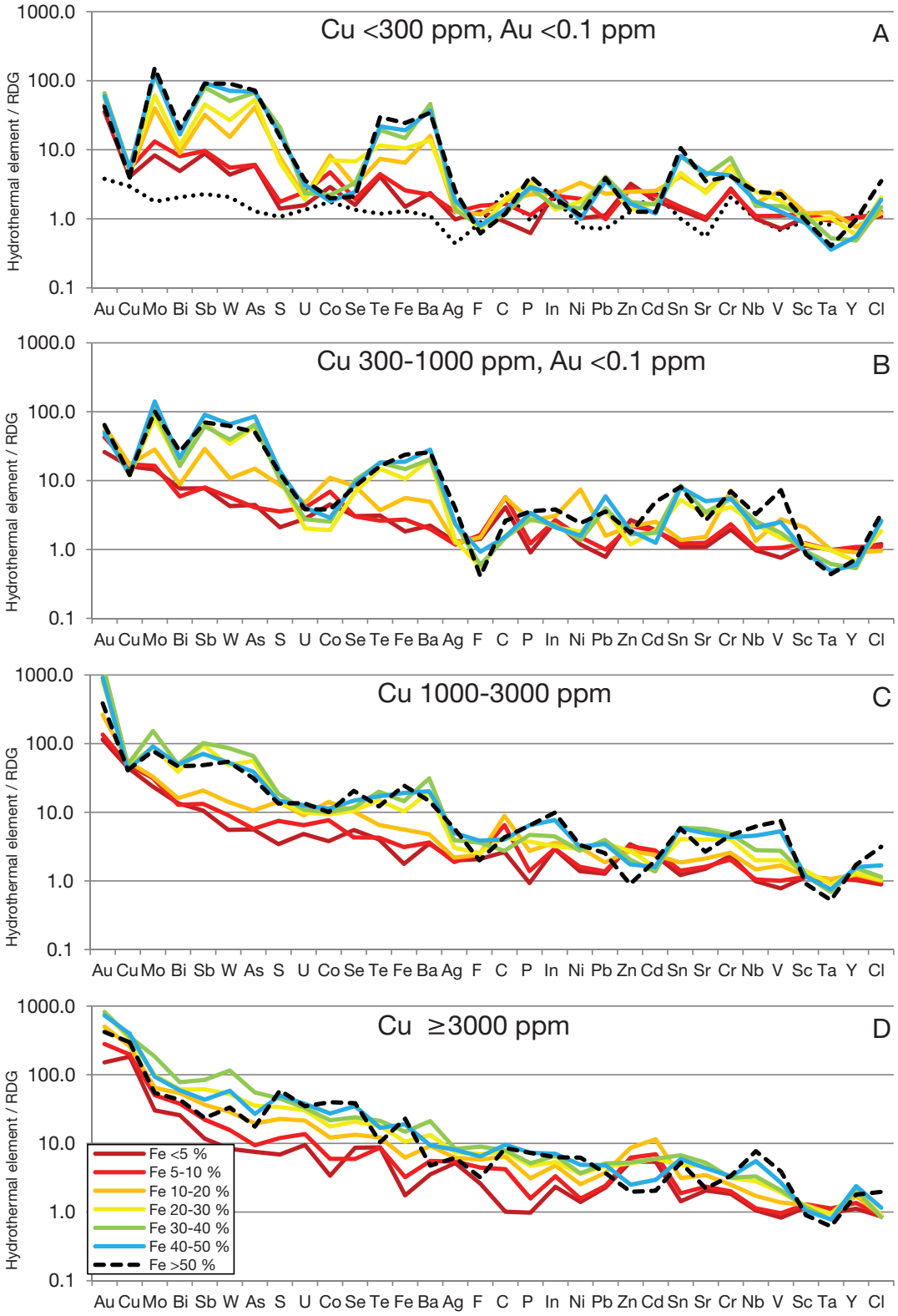


FIG. 12. Hydrothermal-derived (Ag, As, Au, Ba, Bi, Cd, Cl, Co, CO_2, Cr, Cu, F, Fe, In, Mo, Nb, Ni, P, Pb, S, Sb, Sc, Se, Sn, Sr, Ta, Te, U, V, W, Y, and Zn, excluding REE) element mobility for (A) Cu-unmineralized (<300 ppm Cu and <0.1 ppm Au), (B) weakly mineralized (300–1,000 ppm Cu and <0.1 ppm Au), (C) moderately mineralized (1,000–3,000 ppm Cu), and (D) mineralized (≥3,000 ppm Cu) samples. Within each Cu category, conditional means were calculated for each element at increasing Fe concentrations (< 5, 5-10, 10–20, 20–30, 30–40, 40–50, ≥50 wt %). The graphs are the conditional means normalized to the Roxby Downs Granite. The data are from the 10,000-sample MLA dataset. Geochemical trends are discussed in the text.

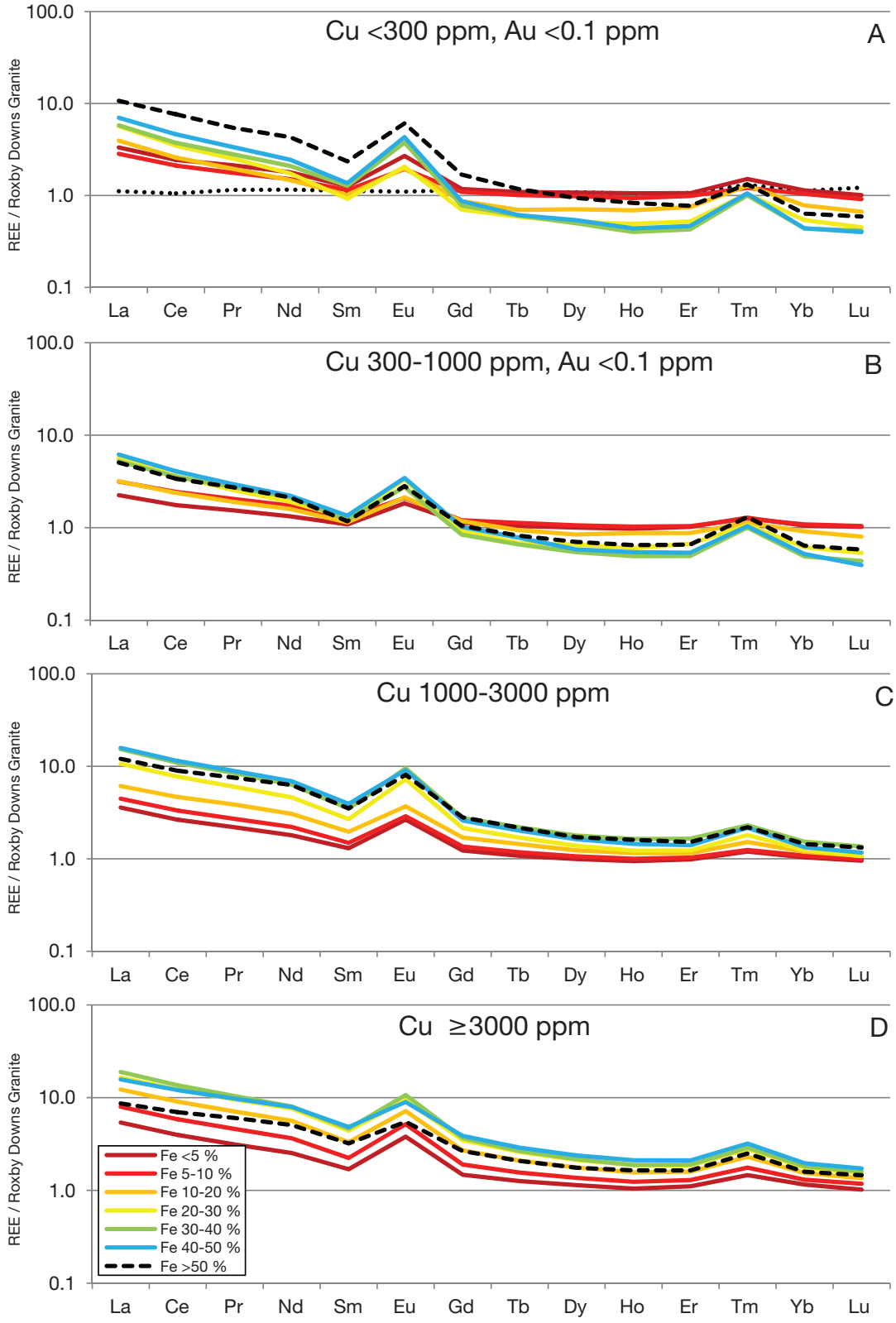


FIG. 13. REE (La, Ce, Pr, Nd, Sm, Eu, Gd, Tb, Dy, Hi, Er, Tm, Yb, Lu) element mobility for (A) Cu-unmineralized (<300 ppm Cu and <0.1 ppm Au), (B) weakly mineralized (300–1,000 ppm Cu and <0.1 ppm Au), (C) moderately mineralized (1,000–3,000 ppm Cu), and (D) mineralized (≥3,000 ppm Cu) samples. Within each Cu category, conditional means were calculated for each element at increasing Fe concentrations (< 5, 5–10, 10–20, 20–30, 30–40, 40–50, ≥50 wt %). The graphs are the conditional means normalized to the Roxby Downs Granite. The data are from the 10,000-sample MLA dataset. Geochemical trends are discussed in the text.

occurs predominantly in barite although it also occurs as a trace constituent in orthoclase. Greater than 99% of the logged sulfide species (at the 1-m scale) occur individually or as the distinct binary pairs mentioned above. Chalcocite has not been observed in contact with chalcopyrite or pyrite; bornite-pyrite pairs are extremely rare and were not observed during logging. The assumptions regarding the sulfide and sulfate mineralogy are sufficiently robust to allow for the quantitative prediction of the absolute wt % of pyrite, chalcopyrite, bornite, and chalcocite in samples based on Cu, S, and Ba assays, which then allows for the 3-D modeling of these sulfide minerals.

The distribution of pyrite-chalcopyrite, chalcopyrite-bornite, and bornite-chalcocite across the deposit is shown in Figure 14A-D. Chalcopyrite is the dominant sulfide mineral across all ore types, with lesser amounts of bornite and chalcocite;

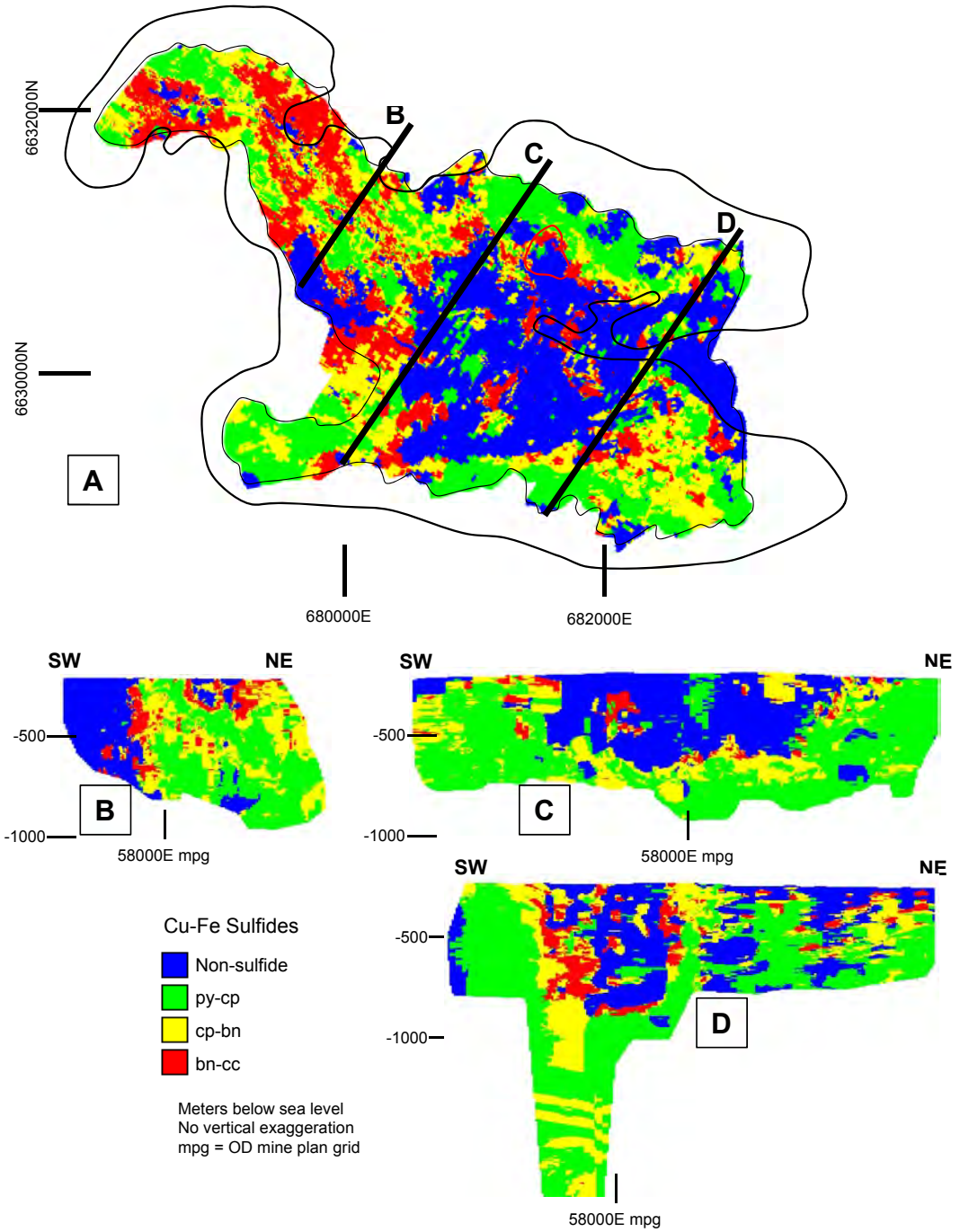


FIG. 14. Simplified chalcopyrite-pyrite, chalcopyrite-bornite, and bornite-chalcocite map at the –350 m RL (A) and cross sections (B-D) of the Olympic Dam Breccia Complex. Chalcopyrite-pyrite is the dominant sulfide pair, with lesser amounts of bornite-chalcocite and chalcopyrite-bornite pairs. The transition from sulfide- to nonsulfide-bearing rock is relatively sharp and follows the metal zonation sequence. Geochemical trends are discussed in the text.

the relative abundances of sulfide pairs is pyrite-chalcopyrite > bornite-chalcocite > chalcopyrite-bornite. There is a sharp transition to nonsulfide bearing rocks.

Siderite, fluorite, and barite zonation

Siderite, fluorite, and barite are zoned across the deposit (Fig. 15). Siderite is typically found at depth and on the deposit edges with magnetite and survives hematite replacement longer than does magnetite. Pyrite and chalcopyrite can be present with siderite, along with fluorite. However, fluorite is more strongly associated hematite alteration and chalcopyrite, bornite, and chalcocite. Barite is strongly associated with hematite in hematite-quartz-barite breccias (very low sulfide) and the rocks immediately surrounding hematite-quartz-barite breccias. Barite occurs with fluorite, chalcopyrite, bornite, and chalcocite. Siderite and barite usually do not occur together, except in late stage barite-fluorite-siderite veins that cut the Olympic Dam Breccia Complex.

Uranium

The uranium minerals do not show any systematic deposit-wide zonation pattern. This is in direct contrast to zonation patterns for sulfides and other minerals. Based on scanning electron microscopy (Fig. 9), the uranium minerals have had a complex history of repeated precipitation, dissolution, and reprecipitation. Overall, uraninite-pitchblende is more strongly associated with hematite and the sulfides, whereas coffinite and brannerite are slightly more associated with the silicates and rutile.

Molybdenum-tin-tungsten and the zone of deep mineralization

RD1988 (1,898-m deep, ending at –1,789 m RL) was drilled near the southeastern margin of the Olympic Dam Breccia Complex (deep drilling on cross sections Figs. 2D, 6D, 15D). The hole ended in 1.6 % Cu, 290 ppm U_3O_8, 1.16 ppm Au, 10 ppm Ag, and 310 ppm Mo. Well-bedded hematite-rich sandstones and mudstones are the dominant rock type to ~825 m (downhole depth), with relict clasts of this rock type in the hematite-rich breccias down to the bottom of the hole. The depth of hematite-rich breccias and mineralization in this hole is the deepest occurrence of significant mineralization and was unexpected because across the deposit, ~50% of the Cu metal occurs above –550 m RL and 90% above –950 m RL (Fig. 16). Analysis for an expanded suite of elements in RD1988 and other nearby shallower holes showed that the area also has elevated concentrations of Mo-As-W-Sn-Sb which are not known to occur elsewhere in the deposit.

Discussion

This section summarizes our new understanding of the geology, hydrothermal alteration, and geochemical plus mineralogical zonation of the Olympic Dam deposit based on the results from resource drilling and the extensive amount of geochemical plus mineralogical data collected from 2003 through 2008. There are numerous metallurgical implications of the mineralogy and mineralogical zonation patterns that have been determined.

Geology

Roxby Downs Granite extends outward from the deposit center for at least 5 to 7 km. Only one other intrusive phase (felsic dike zone in RD2773) has been cut by drilling, in addition to the pre- and synmineralization mafic-ultramafic dikes. Chlorite alteration of igneous biotite (Fig. 1 "biotite-out") is taken to define the outer edge (~1–5 km from deposit center) of the hydrothermal alteration system and the Olympic Dam Breccia Complex. This boundary was previously based on the appearance of plagioclase and unaltered orthoclase (Reeve et al., 1990). There are minor differences between the boundary defined here and by Reeve et al. (1990). The potential for significant mineralization to occur within unaltered Roxby Downs Granite is relatively low.

The bedded clastic facies are the other components within the Olympic Dam Breccia Complex. There has been a gradual evolution in the interpretations of the source and timing of these sediments. Early workers (Reeve et al., 1990; Oreskes and Einaudi, 1990; Johnson and Cross, 1995; Haynes et al., 1995) have interpreted these facies as volcaniclastic units sourced from the Complex and deposited within maar-diatremes (fig. 2A of Reeve et al., 1990), which were synbrecciation and -mineralization. Interestingly, although Bradbury (1988) and Reynolds (2000) depicted a lateral continuity of these units, they favored a maar-diatreme model to explain the bedded clastic facies. McPhie et al. (2011b) interpreted these units as bedded sedimentary facies with a provenance which extended beyond the Olympic Dam area and formed in a sedimentary basin prior to breccia formation and mineralization. The source and timing of these facies remains unresolved but underpins the two major contrasting architecture models of the deposit.

The picrite located in eight drill holes in the basement below the cover sequence has not been previously described. The picrite may represent the source of heat for driving hydrothermal circulation; work is in progress to characterise this picrite. Pre-, syn- and post-mineral mafic and ultramafic dikes occur throughout the Olympic Dam Breccia Complex. The presence of these dikes has been discussed by Krcmarov (1987), Bradbury (1988), Reeve et al. (1990), Johnson and Cross (1995), and Johnson and McCulloch (1995), who proposed that the pre- and synmineral dikes are an integral component of brecciation and mineralization. Mafic dikes are closely associated with mineralization in structurally localized Andean IOCG deposits (Sillitoe, 2003).

Hydrothermal alteration

Progressive destruction of Roxby Downs Granite via Fe oxide addition and sericite alteration of the igneous feldspars can be used to describe hydrothermal alteration system. Based on analyses of whole rock chemistry (Fig. 3) and mineral abundance (Fig. 5) data, alteration zones are clearly defined. Three major transitions (Fig. 6) within the Olympic Dam Breccia Complex are recognized; from the "biotite-out" contour toward the deposit center the transitions are "5 % Fe," "20 % Fe," and sericite-out (or hematite-quartz-barite breccias). These general alteration areas broadly relate to the major breccia types and distribution described by Reeve et al. (1990). However, the transitions in this study are based on

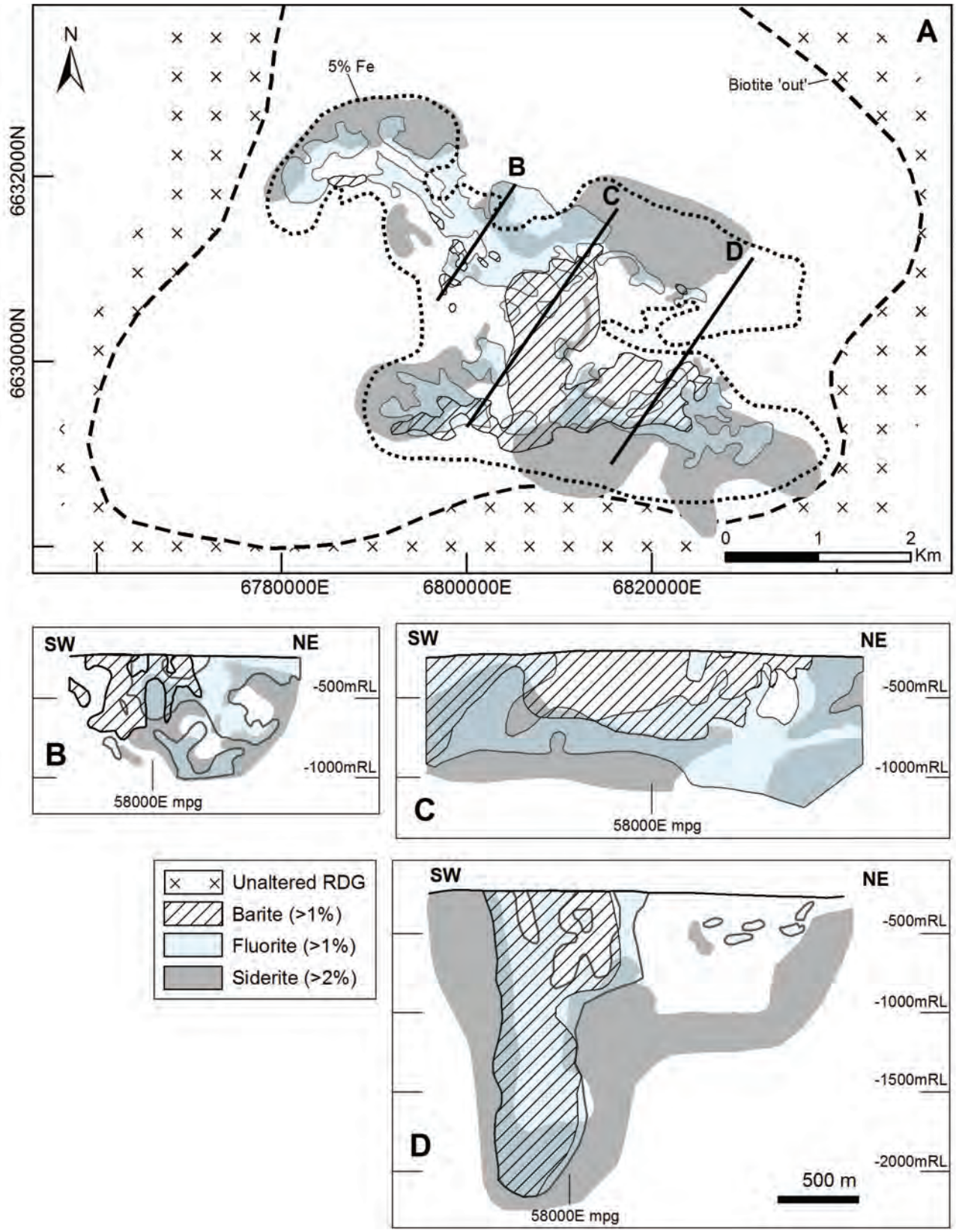


FIG. 15. Simplified barite-fluorite-siderite hydrothermal alteration map at the –350 m RL (A) and cross sections (B-D) of the Olympic Dam Breccia Complex. The deposit is zoned from siderite (at depth and periphery of the deposit) to fluorite to barite (shallow and central parts of the deposit). In general, siderite and barite do not occur together except for late-stage veins that cut the entire deposit; however, overlaps do occur locally.

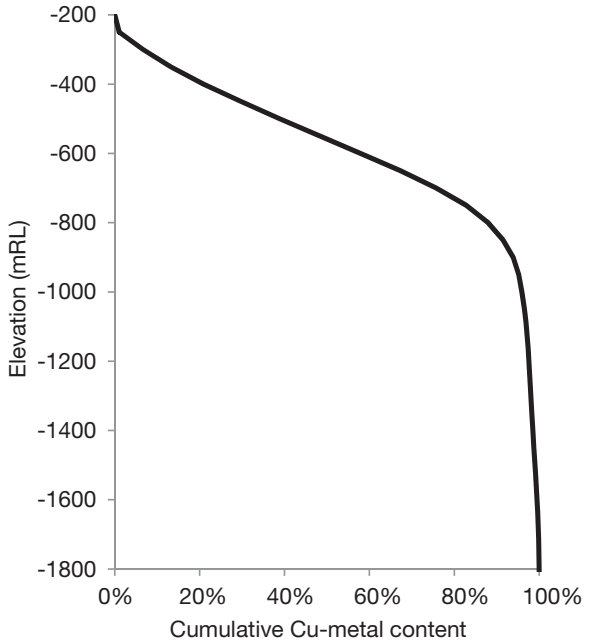


FIG. 16. Cumulative % of Cu metal (above a 0.65% Cu equiv cutoff) with increasing depth. The data are sourced from the 2011 resource model. Approximately 50% of the Cu metal occurs above –550 m RL with ~ 95 % above –950 m RL

measured whole-rock compositional changes, which correlate with changes in mineral abundances, in particular hematite, orthoclase, and sericite.

Reduced Fe oxide (magnetite+apatite+siderite+chlorite +quartz), oxidized Fe oxide (hematite+sericite+fluorite), hematite+quartz+barite, and intense sericitic alteration (sericite +quartz+Al-OH) are the major alteration assemblages. The Fe oxide-bearing assemblages were described by Reeve et al. (1990), Oreskes and Einaudi (1990) and Haynes et al. (1995). Magnetite, siderite, and apatite are now known to be more widespread downward and outward in the deposit than previously documented.

Zunyite, diaspore, and kaolinite locally occur in the intense sericitic alteration areas as isolated pockets; this association may represent relics of advanced argillic alteration that has not been identified previously. These Al-OH minerals, in addition to the widespread occurrence of fluorite (and other F-bearing minerals), and abundant digitate and amoeboid clast shapes (due to hydrothermal dissolution; McPhie et al., 2011b) in the breccia complex are consistent with the evidence for the F- and HF-rich nature of the Olympic Dam hydrothermal system (Oreskes and Einaudi, 1990; McPhie et al., 2011a, b, 2012; Manning, 2012).

Geochemical-mineralogical zonation

Based on assays of individual drill core samples, strong correlations exist between whole-rock iron and a wide suite of elements and minerals (Figs. 3, 5, 7, 10–13). Iron concentration is zoned across the deposit (Fig. 2), so by inference elements and minerals which are strongly correlated with Fe concentration are also zoned across the deposit. The best examples are orthoclase-sericite (Fig. 6), pyrite-chalcopyrite-bornite-chalcocite (Fig. 14), and siderite-fluorite-barite (Fig. 15). No assessment has yet been made regarding element mass gains or losses.

Chalcopyrite is the dominant Cu sulfide and chalcopyrite-pyrite is the principal sulfide assemblage; the other major sulfide assemblages are bornite-chalcocite followed by chalcopyrite-bornite. Sphalerite and galena occur in the extreme northwest and southeast areas, on the deposit margins, which demonstrates the presence of deposit-wide Cu-Pb-Zn zonation. Copper sulfide mineralization below –950 mRL exists in the southeastern part of the deposit (Figs. 2D, 6D, 14D, 15D). A base metal-poor signature (Mo-As-W-Sn-Sb) is associated with and surrounding the –950 mRL mineralized area, and with Cu-unmineralized (<300 ppm Cu; Fig 12A) and weakly mineralized (300–1,000 ppm Cu: Fig. 12B) samples. This occurrence of elevated concentrations of Mo-As-W-Sn-Sb may represent a deeper distal and/or paragenetically earlier style of mineralization.

Coffinite is the dominant uranium mineral (Fig. 10); Hayward and O'Connell (2007) also reported coffinite as the major uranium bearing mineral based on an in-progress version of the 10,000-sample MLA dataset at that time. However, it is now apparent that the relative proportion of uraninite compared with coffinite and brannerite increases with increasing whole-rock Fe concentration. Roberts and Hudson (1983), Reeve et al. (1990), Oreskes and Einaudi (1990), and Reynolds (2000) all reported uraninite/pitchblende as the principal uranium mineral which was based on relatively limited microscopic characterisation of the uranium minerals in early days.

Metallurgical implications of geochemical and mineralogical zonation

All major base metal ore deposits have variable alteration and mineralization patterns across the deposit, which means that as a deposit is mined the characteristics of the ore will change with time because of the mineralogical variation. At Olympic Dam, every block in the resource model (>20 M blocks varying in size from 5 × 10 × 5 m up to 30 × 30 × 15 m) has 26 elements, bulk dry density, lithology, and 12 minerals that are necessary to mathematically describe the quantitative relationships that link metallurgical performance (i.e., throughputs, recoveries, and reagent consumptions) to ore composition and mineralogy. This is a powerful dataset because metallurgical performance can be calculated and potential economic return can be evaluated on every block in the resource model. This geometallurgy-enabled resource block model is then used for short-, medium- and long-term mine planning, process plant design, and optimizations. Without quantifying mineral abundances across the entire deposit and resource model, predicting the mineralogical, metallurgical performance and potential economic return of future plant feed at Olympic Dam would not be possible.

Based on almost 25 years of mining and processing ore at Olympic Dam, the following minerals and elements have been determined to be important indicators of processing performance: (1) hematite, quartz, and sericite wt % (mill throughput and power consumption); (2) pyrite, chalcopyrite, bornite, and chalcocite wt % in plant feed (copper concentrate grade); (3) U_3O_8 grade, wt % of uraninite, coffinite, and brannerite (variable leaching rates), and chlorite and siderite

wt % (uranium recovery); (4) chlorite and siderite wt % (acid consumption); (5) chlorite wt % (U_3O_8 leach circuit gelling potential); (6) sericite wt % (settling, i.e., solid-liquid separation); (7) pyrite, chalcopyrite, bornite, chalcocite, hematite, quartz, and sericite wt % (smelter throughput); and (8) Pb, Zn, As, Se, Te, Bi, and Sb wt % (copper cathode quality).

Conclusions

The ore and gangue minerals at Olympic Dam are systematically distributed across the deposit, but the resulting zonation patterns are difficult to identify based on logging and mapping alone because of the intense texturally destructive Fe oxide and sericite alteration and brecciation of the Roxby Downs Granite, bedded clastic facies, and pre- and synmineral mafic and ultramafic dikes. However, when logging and mapping are combined with mineralogical and geochemical data, the style and distribution of alteration and mineralization become increasingly predictable.

The elements can be grouped according to their correlation with whole-rock Fe concentration: (1) Roxby Downs Granite-derived (Al, Be, Ca, Hf, K, Li, Mg, Mn, Na, Rb, Si, Th, Ti, and Zr) are negatively correlated, (2) hydrothermal elements (Ag, As, Au, Ba, Bi, Cd, Cl, Co, C, Cr, Cu, F, In, Mo, Nb, Ni, P, Pb, S, Sb, Sc, Se, Sn, Sr, Ta, Te, U, V, W, Y and Zn) are positively correlated, and (3) REE (La, Ce, Pr, Nd, Sm, Eu, Gd, Tb, Dy, Ho, Er, Tm, Yb, Lu) are also positively correlated. The ore and gangue minerals are also correlated with Fe. There is a strong spatial association of Cu, U_3O_8, Au, and Ag.

Three hydrothermal alteration assemblages record the transition (from deposit margin to center) from Fe^{+2} to Fe^{+3}- and sulfide to sulfate-dominated conditions; relatively reduced Fe oxide alteration (magnetite+apatite+siderite+chlorite+quartz) to oxidized Fe oxide alteration (hematite+sericite+fluorite), and hematite+quartz+barite alteration. Remnants of advanced argillic alteration (sericite+quartz ± Al-OH) are also present.

The well-established Cu-Fe sulfide zonation can be extended to include Pb and Zn; from the deposit periphery toward the center, the zonation is sphalerite → galena → pyrite → chalcopyrite → bornite → chalcocite → nonsulfide. There is also new evidence for a distal and deep or paragenetically early, base metal-poor (Mo-W-Sn-As-Sb) enrichment which may be overprinted by Cu-Pb-Zn.

Acknowledgments

Over 100 geoscientists have worked at Olympic Dam since discovery and have contributed materially to this manuscript via routine diligent logging of diamond drill core and mapping of underground exposures; the contribution of mine-based geoscientists should never be underestimated. We gratefully acknowledge Ken Cross for openly sharing his ideas and observations over the years, Guy Dishaw and Felipe Urzúa for their structural work, Shane O'Connell and Colin Badenhorst for the enormous effort involved in producing over 40 block models of various elements and minerals, Edeltraud Macmillan and Chantelle Lower for the endless requests for sections and plans and Antonio Arribas for drafting support. Jon Gilligan (geologist), Ken Sutliff (metallurgist), and Barry Mitchell (mining engineer) ensured that the budget and other support were available for collection of the comprehensive geochemical and mineralogical data sets. The authors wish to thank BHP Billiton for permission to publish this paper. Jeff Hedenquist, Mike Harris, and Antonio Arribas encouraged completion of this manuscript. Exhaustive, constructive reviews from Jeff, Mike, Lucas Marshall, and an anonymous reviewer were extremely helpful in improving the quality of this manuscript. KJE would like to acknowledge Roy Woodall (Director of Exploration for WMC) for being a mentor and providing boundless enthusiasm and moral support to those who document the geology of the deposits that we, as an industry, exploit.

REFERENCES

Allen, S.R. and McPhie, J., 2002, The Eucarro Rhyolite, Gawler Range Volcanics, South Australia: A >675 km^3 compositionally zoned felsic lava of Mesoproterozoic age: Geological Society of America Bulletin, v. 114, p. 1592–1609.

Allen, S.R., Simpson, C.J., McPhie, J. and Daly, S.J., 2003, Stratigraphy, distribution and geochemistry of widespread felsic volcanic units in the Mesoproterozoic Gawler Range Volcanics, South Australia: Australian Journal of Earth Sciences, v. 50, p. 97–112.

Allen, S.R., McPhie, J., Ferris, G., and Simpson, C., 2008, Evolution and architecture of a large felsic igneous province in western Laurentia: The 1.6 Ga Gawler Range Volcanics, South Australia: Journal of Volcanology and Geothermal Research, v. 172, p. 132–147.

BHP Billiton, 2012, Annual report 2012: http://www.bhpbilliotn.com/home/investors/reports/Documents/2012/BHPBillitonAnnualReport2012.pdf.

Blissett, A.H., Creaser, R.A., Daly, S.J, Flint, D.J., and Parker, A.J., 1993, Gawler Range Volcanics, *in* Drexel, J. F., Preiss, W.V., and Parker, A.J., eds., The geology of South Australia. Volume 1, The Precambrian: Adelaide, Geological Survey of South Australia, Bulletin 54, p. 107–131.

Bradbury, J., 1988, The volcanic and shallow sub-volcanic component of the breccias hosted Olympic Dam U-Cu-Au deposit: Implication for breccias pipe development: Unpublished B.Sc. (Honours) thesis, Melbourne, Australia, Monash University, 134 p.

Cowley, W.M., 1991, The Pandurra Formation: Department of Mines and Energy South Australia, Adelaide, Report Book 91/7, 45 p.

Creaser, R., 1989, The geology and petrology of Middle Proterozoic felsic magmatism of the Stuart Shelf, South Australia: Unpublished Ph.D. thesis, Bundoora, Australia, La Trobe University, 434 p.

Fanning, C.M., Flint, R.B., and Preiss, W.V., 1983, Geochronology of the Pandurra Formation: Geological Survey of South Australia Quarterly Geological Notes, v. 88, p. 11–16.

Fanning, C.M., Blissett, R.B., Parker, A.J., Ludwig, K.R., and Blissett, A.H., 1988, Refined Proterozoic evolution of the Gawler Craton, South Australia, through U-Pb geochronology: Precambrian Research, v. 40/41, p. 363–386.

Flint, R.B., Blissett, A.H., Conor, C.H.H., Cowley, W.M., Cross, K.C., Creaser, R.A., Daly, S.J., Krieg, G.W., Major, R.B., Teale, G.S., and Parker, A.J., 1993, Mesoproterozoic, *in* Drexel, J.F., Preiss, W.V., and Parker, A.J., eds., The geology of South Australia; Volume 1, The Precambrian: Adelaide, Geological Survey of South Australia, Bulletin 54, p. 106–169.

Giles, C.W., 1988, Petrogenesis of the Proterozoic Gawler Range Volcanics, South Australia: Precambrian Research, v. 40/41, p. 407–427.

Gu, Y., 2003, Automated scanning electron microscope based mineral liberation analysis: Journal of Minerals & Materials Characterization & Engineering, v. 2, p. 33–41.

Hand, M., Reid, A., and Jagodzinski, E., 2007, Tectonic framework and evolution of the Gawler Craton, South Australia: Economic Geology, v. 102, p. 1377–1395.

Haynes, D.W., Cross, K.C., Bills, R.T., and Reed, M.H., 1995, Olympic Dam ore genesis; a fluid-mixing model: Economic Geology, v. 90, p. 281–307.

Hayward, N., and Skirrow, R., 2010, Geodynamic setting and controls on iron oxide Cu-Au (±U) ore in the Gawler Craton, South Australia, *in* Porter, T. M., ed., Hydrothermal iron oxide copper-gold and related deposits: A global perspective, volume 3, Advances in the understanding of IOCG deposits: Adelaide, PGC Publishing, p. 105–131.

Hayward, S., and O'Connell, S., 2007, Mineral resource estimation at Olympic Dam: Presentations, Uranium Reporting Workshop, Uranium and the JORC Code, Adelaide, 28 November 2007, Australasian Institute of Mining and Metallurgy, Melbourne.

Hemley, J.J., Montoya, J.W., Marinenko, J.W., and Luce, R.W., 1980, Equilibria in the system Al_2O_3-SiO_2-H_2O and some general implications for alteration-mineralization processes: Economic Geology, v. 75, p. 210–228.

Hoatson, D., Claoué-Long, J., and Jaireth, S., 2008, Proterozoic mafic-ultramafic magmatism in Australia: Geological settings and metallogeny: Australian Nickel Conference, 22–23rd October 2008, Geoscience Australia. (PowerPoint presentation downloaded from http://www.ga.gov.au/image_cache/GA12488.pdf).

Johnson, J.P., and Cross, K.C., 1995, U-Pb geochronological constraints on the genesis of the Olympic Dam Cu-U-Au-Ag deposit, South Australia: Economic Geology, v. 90, p. 1046–1063.

Johnson, J.P., and McCulloch, M.T., 1995, Sources of mineralising fluids for the Olympic Dam deposit (South Australia): SM-Nd isotopic constraints: Chemical Geology, v. 121, p. 177–199.

Krcmarov, R., 1987, The geology, petrology and geochemistry of the volcanic unit at Olympic Dam, South Australia: Unpublished B.Sc. (Honours) thesis, Adelaide, Australia, The University of Adelaide, 106 p.

Manning, D.A.C., 2012, The fluorine link between a supergiant ore deposit and a silicic large igneous province: Comment: Geology, v. 40, e275, doi:10.1130/G33040C.1.

McPhie, J., Della Pasqua, F., Allen, S.R., and Lackie, M., 2008, Extreme effusive eruptions: palaeoflow data on an extensive felsic lava in the Mesoproterozoic Gawler Range Volcanics: Journal of Volcanology and Geothermal Research, v. 172, p. 148–161.

McPhie, J., Kamenetsky, V., Allen, S.R., Ehrig, K., Agangi, A., and Bath, A., 2011a, The fluorine link between a supergiant ore deposit and a silicic large igneous province: Geology, v. 39, p. 1003–1006.

McPhie, J., Kamenetsky, V., Chambefort, I., Ehrig, K., and Green, N., 2011b, Origin of the supergiant Olympic Dam Cu-U-Au-Ag deposit, South Australia: Was a sedimentary basin involved?: Geology, v. 39, p. 795–798.

McPhie, J., Kamenetsky, V., Allen, S.R., Ehrig, K., Agangi, A., and Bath, A., 2012, The fluorine link between a supergiant ore deposit and a silicic large igneous province: Reply: Geology, v. 40, e276, doi: 10.1130/G33378Y.1.

O'Driscoll, E.S.T., 1985, The application of lineament tectonics in the discovery of the Olympic Dam Cu-Au-U deposit at Roxby Downs, South Australia: Global Tectonics and Metallogeny, v. 3, p. 43–57.

Oreskes, N., and Einaudi, M.T., 1990, Origin of rare earth element-enriched hematite breccias at the Olympic Dam Cu-U-Au-Ag deposit, Roxby Downs South Australia: Economic Geology, v. 85, p. 1–85.

——1992, Origin of hydrothermal fluids at Olympic Dam: Preliminary results from fluid inclusions and stable isotopes: Economic Geology, v. 87, p. 64–90.

Preiss, W.V., 1993, Neoproterozoic, *in* Drexel, J.F., Preiss, W.V., and Parker, A.J., eds., The geology of South Australia; Volume 1, The Precambrian: Adelaide, Geological Survey of South Australia, Bulletin 54, p. 170–203.

Reeve, J.S., 1990a, The discovery and evaluation of the Olympic Dam deposit, *in* Glasson, K.R., Rattigan, J.H., eds., Geological aspects of the discovery of some important mineral deposits in Australia: Australasian Institute of Mining and Metallurgy, Monograph 17, p. 125–133.

——1990b, The discovery and evaluation of gold mineralization within the Olympic Dam deposit, South Australia, *in* Glasson, K.R., Rattigan, J.H., eds., Geological aspects of the discovery of some important mineral deposits in Australia: Australasian Institute of Mining and Metallurgy, Monograph 17, p. 57–58.

Reeve, J.S., Cross, K.C., Smith, R.N., and Oreskes, N., 1990, Olympic Dam copper-uranium-gold-silver deposit, *in* Hughes, F.E., ed., Geology of the Mineral Deposits of Australia and Papua New Guinea: Australasian Institute of Mining and Metallurgy, Monograph 14, p. 1009–1035.

Reid, A.J., Fricke, C.E., and Cowley, W.M., 2009, Extent of low-grade Archaean metavolcanics in the northeastern Gawler Craton: New evidence and definition of the Devils Playground Volcanics: MESA Journal, v. 54, p. 9–19.

Reynolds, L.J, 2000, Geology of the Olympic Dam Cu-U-Au-Ag-REE deposit, *in* Porter, T. M., ed., Hydrothermal iron oxide copper-gold and related deposits: A global perspective, volume 1, Adelaide, Porter Publishing, p. 93–104.

Roache, M.W., Allen, S.R., and McPhie, J., 2000, Surface and subsurface facies architecture of a small hydroexplosive, rhyolitic centre in the Mesoproterozoic Gawler Range Volcanics, South Australia: Journal of Volcanology and Geothermal Research, v. 104, p. 237–259.

Roberts, D.E., and Hudson, G.R.T., 1983, The Olympic Dam copper-uranium-gold deposit, Roxby Downs, South Australia: Economic Geology, v. 78, p. 799–822.

Sillitoe, R.H., 2003, Iron oxide-copper-gold deposits: an Andean view: Mineralium Deposita, v. 38, p. 787–812.

Sugden, T.J, and Cross, K.C., 1991, Significance of the overprinting fault systems in the Olympic Dam Breccia Complex: University of Western Australia, Geology Department and University Extension, Publication 25, p. 93–98.

Widdup, H., Fouet, T., Hodgkison, J., McCuaig, T.C., and Miller, J., 2004, A three-dimensional structural interpretation of the Olympic Dam deposit—implications for mine planning and exploration: Hi Tech and World Competitive Mineral Success Stories Around the Pacific Rim, Proceedings of the Pacrim 2004 Conference, Adelaide, 19–22 September, 2004, Australasian Institute of Mining and Metallurgy, Melbourne, p. 417–426.

Woodall, R., 1994, Empiricism and concept in successful mineral exploration: Australian Journal of Earth Sciences, v. 4, p. 1–10.

Zhao, J.X., and McCulloch, M.T., 1993, Sm-Nd mineral isochron ages of Late Proterozoic dyke swarms in Australia: Evidence for two distinct events of mafic magmatism and crustal extension: Chemical Geology, v. 109, p. 341–354.

Zhao, J.X., McCulloch, M.T., and Korsch, R.J., 1994, Characterisation of a plume-related ~ 800 Ma magmatic event and its implications for basin formation in central-southern Australia: Earth and Planetary Science Letters, v. 121, p. 349–367.

APPENDIX

TABLE A1. Conditional Means of RDG, RDG-Sericite-Altered, and Cu-Unmineralized Samples[1]

		RDG	RDG-ser alt	Unmineralized samples (Cu <300 ppm, Au <0.1 ppm)						
		n = 49	n = 68	<5% Fe n = 154	5–10% Fe n = 76	10–20% Fe n = 81	20–30% Fe n = 78	30–40% Fe n = 66	40–50% Fe n = 90	≥50% Fe n = 89
SiO_2	(wt %)	69.6	69.3	72.4	68.8	64.8	57.1	38.6	26.8	9.24
TiO_2	(wt %)	0.43	0.39	0.28	0.35	0.33	0.31	0.28	0.14	0.12
Al_2O_3	(wt %)	13.37	13.41	13.08	12.73	5.46	1.74	1.93	0.91	0.35
Fe_2O_3	(wt %)	3.37	4.34	5.03	8.70	21.9	35.3	49.6	64.4	81.8
MnO	(wt %)	0.08	0.09	0.02	0.05	0.05	0.05	0.03	0.03	0.03
MgO	(wt %)	0.83	0.64	0.35	0.56	0.60	0.51	0.36	0.22	0.27
CaO	(wt %)	0.85	0.52	0.15	0.30	0.40	0.50	0.39	0.42	0.37
Na_2O	(wt %)	3.40	1.50	0.15	0.16	0.10	0.09	0.09	0.08	0.13
K_2O	(wt %)	5.53	6.94	5.20	5.21	1.74	0.38	0.52	0.23	0.04
P_2O_5	(wt %)	0.07	0.07	0.05	0.08	0.17	0.25	0.21	0.21	0.31
CO_2	(wt %)	0.27	0.68	0.24	0.44	0.49	0.52	0.32	0.37	0.32
S	(wt %)	0.05	0.05	0.06	0.08	0.36	0.30	0.97	0.78	0.71
F	(wt %)	0.19	0.17	0.24	0.29	0.22	0.13	0.15	0.15	0.12
Cl	(ppm)	346	440	374	434	416	702	508	651	1216
Cu	(ppm)	38	113	156	204	173	194	206	202	152
U_3O_8	(ppm)	13	18	21	32	27	25	31	41	47
Au	(ppb)	0.8	3.0	28.0	34.6	49.4	43.5	52.2	47.3	32.8
Ag	(ppm)	0.3	0.1	0.3	0.4	0.4	0.5	0.4	0.6	0.8
As	(ppm)	4.9	6.3	29	30	203	262	330	340	354
Bi	(ppm)	0.1	0.2	0.5	0.9	1.0	1.3	1.9	1.8	2.3
Cd	(ppm)	0.1	0.2	0.1	0.2	0.2	0.1	0.1	0.1	0.1
Co	(ppm)	4.3	7.5	12.3	20.1	35.1	30.2	9.5	7.6	8.4
In	(ppm)	0.0	0.1	0.1	0.1	0.1	0.0	0.1	0.1	0.1
Mo	(ppm)	0.9	1.6	7.4	11.8	35.6	54.5	106.7	114.6	137.0
Ni	(ppm)	2.8	2.1	2.8	5.4	9.3	5.0	4.0	2.8	3.1
Pb	(ppm)	14.3	10.2	16.0	14.0	32.7	50.4	57.8	50.1	55.3
Sb	(ppm)	0.3	0.8	3.1	3.3	11.1	15.6	27.5	31.9	31.2
Se	(ppm)	0.3	0.3	0.4	0.5	0.8	1.7	0.8	0.6	0.5
Te	(ppm)	0.1	0.1	0.5	0.6	0.9	1.4	2.4	2.7	3.7
Tl	(ppm)	0.6	0.9	0.6	0.7	0.7	0.2	0.2	0.1	0.1
Zn	(ppm)	41	52	130	112	100	54	71	67	51
Ba	(wt %)	0.09	0.09	0.20	0.19	1.36	1.17	3.93	3.15	2.93
Be	(ppm)	4.6	4.1	2.4	3.0	2.3	2.0	1.0	1.2	1.1
Cr	(ppm)	10	21	27	26	58	54	76	42	41
Cs	(ppm)	2.0	2.7	2.7	3.3	2.1	0.6	0.8	0.3	0.1
Ga	(ppm)	20.3	23.8	24.4	22.8	15.8	9.8	8.5	7.5	8.3
Hf	(ppm)	10.3	9.4	8.6	9.4	8.8	7.9	5.5	3.0	2.1
Li	(ppm)	19	10	12	13	13	8	8	4	3
Nb	(ppm)	31	31	31	34	52	76	47	55	76
Rb	(ppm)	258	320	199	199	78	15	24	10	1
Sc	(ppm)	2.9	2.7	3.1	3.5	3.5	2.8	3.3	2.5	2.7
Sn	(ppm)	7	7	9	10	28	32	55	56	72
Sr	(ppm)	91	50	87	94	228	215	385	417	317
Ta	(ppm)	2.9	2.3	2.7	2.7	3.6	3.0	1.5	1.0	1.2
Th	(ppm)	52	61	65	56	31	30	25	12	11
V	(ppm)	15	11	11	17	39	28	24	19	35
W	(ppm)	2	5	10	13	36	63	120	168	213
Y	(ppm)	46	54	49	47	35	27	22	25	45
Zr	(ppm)	338	346	274	310	290	281	182	99	80
La	(ppm)	0.01	0.01	0.03	0.03	0.04	0.05	0.06	0.07	0.10
Ce	(ppm)	0.02	0.02	0.05	0.04	0.05	0.07	0.07	0.09	0.15
Pr	(ppm)	21	24	45	37	41	53	59	71	115
Nd	(ppm)	70	80	124	105	102	121	146	170	300
Sm	(ppm)	12.4	14.0	15.7	14.2	12.6	11.5	15.9	17.0	29.2
Eu	(ppm)	1.7	1.9	4.7	3.3	3.4	3.6	6.5	7.5	10.5
Gd	(ppm)	10.3	11.8	12.2	11.3	9.0	7.3	8.0	9.0	17.4
Tb	(ppm)	1.6	1.7	1.8	1.6	1.1	0.9	1.0	1.0	1.9
Dy	(ppm)	9.5	10.3	10.2	9.3	6.7	4.9	4.7	5.1	8.9
Ho	(ppm)	1.9	2.0	2.0	1.8	1.3	0.9	0.8	0.8	1.6
Er	(ppm)	5.7	6.1	6.0	5.6	4.3	3.0	2.4	2.7	4.4
Tm	(ppm)	0.5	0.7	0.8	0.6	0.6	0.5	0.5	0.5	0.7
Yb	(ppm)	5.6	6.3	6.4	5.8	4.4	3.0	2.4	2.5	3.5
Lu	(ppm)	0.9	1.1	0.9	0.9	0.6	0.4	0.4	0.4	0.6

[1] Samples from the 10,000-sample MLA data set; all analyses conducted at AMDEL-Bureau Veritas, Adelaide

TABLE A2. Conditional Means Cu Weakly Mineralized Samples[1]

		Weakly mineralized samples (Cu <1,000 ppm, Au <0.1 ppm)						
		< 5 % Fe n = 35	5–10 % Fe n = 59	10–20% Fe n = 116	20–30% Fe n = 123	30–40% Fe n = 84	40–50% Fe n = 78	≥50% Fe n = 87
SiO_2	(wt %)	69.1	66.8	59.7	56.1	42.7	27.5	12.1
TiO_2	(wt %)	0.35	0.37	0.36	0.31	0.29	0.27	0.13
Al_2O_3	(wt %)	12.96	12.63	10.52	1.72	1.64	1.39	0.55
Fe_2O_3	(wt %)	6.14	9.16	18.9	35.6	49.5	63.4	80.3
MnO	(wt %)	0.09	0.13	0.12	0.04	0.04	0.04	0.05
MgO	(wt %)	0.38	0.51	0.73	0.23	0.32	0.36	0.41
CaO	(wt %)	0.22	0.24	0.38	0.41	0.39	0.50	0.66
Na_2O	(wt %)	0.17	0.15	0.12	0.09	0.11	0.10	0.13
K_2O	(wt %)	6.74	5.68	3.68	0.46	0.43	0.32	0.10
P_2O_5	(wt %)	0.07	0.09	0.20	0.22	0.20	0.25	0.27
CO_2	(wt %)	1.10	1.54	1.53	0.43	0.40	0.41	0.70
S	(wt %)	0.10	0.16	0.39	0.49	0.47	0.63	0.58
F	(wt %)	0.27	0.31	0.28	0.11	0.11	0.18	0.08
Cl	(ppm)	414	384	330	643	912	885	1140
Cu	(ppm)	614	661	656	456	458	482	466
U_3O_8	(ppm)	37	53	63	27	36	53	50
Au	(ppb)	20.5	33.5	48.8	41.1	40.7	38.2	50.8
Ag	(ppm)	0.4	0.4	0.4	0.4	0.8	0.8	1.3
As	(ppm)	21.8	20.0	73.3	298	320	421	249
Bi	(ppm)	0.8	0.6	1.0	1.9	1.8	2.3	2.9
Cd	(ppm)	0.1	0.1	0.2	0.1	0.1	0.1	0.3
Co	(ppm)	19.2	29.5	46.8	8.2	10.9	12.3	16.3
In	(ppm)	0.1	0.1	0.1	0.1	0.1	0.1	0.1
Mo	(ppm)	12.9	14.6	25.3	72.3	93.6	125.5	90.0
Ni	(ppm)	3.3	4.2	20.8	5.1	3.8	4.4	6.7
Pb	(ppm)	11.1	14.2	22.6	53.6	56.8	84.6	50.8
Sb	(ppm)	2.7	2.7	9.9	23.7	21.2	31.0	24.1
Se	(ppm)	0.8	0.8	2.1	1.7	2.5	2.3	2.1
Te	(ppm)	0.4	0.3	0.5	1.9	2.3	2.3	2.0
Tl	(ppm)	0.7	0.6	0.6	0.3	0.2	0.2	0.1
Zn	(ppm)	109	89	88	48	67	76	71
Ba	(wt %)	0.19	0.17	0.42	1.78	1.74	2.40	2.20
Be	(ppm)	2.3	2.8	3.2	1.5	1.7	1.3	1.6
Cr	(ppm)	19	23	72	42	54	55	70
Cs	(ppm)	2.4	2.5	3.6	0.8	0.5	0.4	0.3
Ga	(ppm)	22.6	22.6	20.6	11.9	9.7	9.3	6.6
Hf	(ppm)	9.5	9.8	8.6	7.9	6.8	5.2	2.3
Li	(ppm)	10	12	14	5	6	7	6
Nb	(ppm)	30	32	41	71	79	64	100
Rb	(ppm)	240	210	154	24	23	15	5
Sc	(ppm)	3.4	3.6	6.0	3.5	2.8	2.6	2.5
Sn	(ppm)	7	8	9	36	58	54	56
Sr	(ppm)	99	113	138	291	314	456	241
Ta	(ppm)	2.8	2.8	2.8	2.8	1.8	1.4	1.3
Th	(ppm)	60	58	42	31	30	21	11
V	(ppm)	12	16	43	23	27	39	112
W	(ppm)	10	13	25	80	93	155	146
Y	(ppm)	48	50	42	31	25	28	33
Zr	(ppm)	320	330	272	250	221	182	71
La	(ppm)	0.02	0.03	0.03	0.05	0.05	0.06	0.05
Ce	(ppm)	0.03	0.05	0.05	0.07	0.07	0.08	0.06
Pr	(ppm)	33	43	40	54	58	63	58
Nd	(ppm)	92	120	111	132	148	154	148
Sm	(ppm)	13.5	15.9	14.2	15.9	15.2	16.8	14.6
Eu	(ppm)	3.2	3.6	3.7	5.8	4.8	6.0	4.9
Gd	(ppm)	11.7	12.4	12.2	9.6	8.7	10.5	10.8
Tb	(ppm)	1.7	1.8	1.5	1.1	1.1	1.3	1.3
Dy	(ppm)	9.5	10.0	8.0	6.2	5.2	5.5	6.7
Ho	(ppm)	1.8	1.9	1.7	1.1	0.9	1.0	1.2
Er	(ppm)	5.8	5.9	5.0	3.8	2.8	3.1	3.7
Tm	(ppm)	0.6	0.6	0.6	0.5	0.5	0.5	0.7
Yb	(ppm)	5.9	6.1	5.1	3.4	2.7	2.9	3.6
Lu	(ppm)	1.0	1.0	0.8	0.5	0.4	0.4	0.5

[1] Samples from the 10,000-sample MLA data set; all analyses conducted at AMDEL-Bureau Veritas, Adelaide

TABLE A3. Conditional Means Cu Moderately Mineralized Samples[1]

		Moderately mineralized samples (Cu 1,000-3,000 ppm)						
		<5% Fe n = 176	5–10% Fe n = 867	10–20% Fe n = 310	20–30% Fe n = 100	30–40% Fe n = 54	40–50% Fe n = 32	≥50% Fe n = 42
SiO_2	(wt %)	69.1	65.0	58.4	47.5	34.5	22.4	7.92
TiO_2	(wt %)	0.34	0.35	0.33	0.33	0.24	0.11	0.06
Al_2O_3	(wt %)	12.96	12.15	10.82	7.25	4.65	2.57	1.09
Fe_2O_3	(wt %)	5.98	10.5	18.9	34.5	48.8	64.6	82.8
MnO	(wt %)	0.06	0.13	0.19	0.09	0.07	0.08	0.10
MgO	(wt %)	0.33	0.45	0.60	0.68	0.86	0.56	0.51
CaO	(wt %)	0.37	0.46	0.51	0.69	1.15	1.55	1.17
Na_2O	(wt %)	0.17	0.14	0.12	0.12	0.08	0.09	0.11
K_2O	(wt %)	6.39	5.64	4.07	2.20	1.23	0.60	0.18
P_2O_5	(wt %)	0.07	0.10	0.20	0.28	0.35	0.48	0.48
CO_2	(wt %)	0.71	1.75	2.38	1.16	0.74	1.08	1.16
S	(wt %)	0.16	0.34	0.65	0.65	0.86	0.68	0.62
F	(wt %)	0.39	0.47	0.46	0.48	0.68	0.73	0.38
Cl	(ppm)	308	326	348	360	396	582	1088
Cu	(ppm)	1713	1886	2111	1855	1889	1565	1579
U_3O_8	(ppm)	64	86	119	132	144	166	179
Au	(ppb)	90.8	107.4	208.4	639.0	1131.3	723.9	305.2
Ag	(ppm)	0.7	0.6	0.7	1.0	1.3	1.7	1.9
As	(ppm)	27.7	28.2	52.4	275	324	191	154
Bi	(ppm)	1.5	1.4	1.8	4.3	5.5	5.5	5.1
Cd	(ppm)	0.2	0.2	0.2	0.1	0.1	0.1	0.1
Co	(ppm)	16.1	32.7	60.6	39.6	42.7	48.1	42.8
In	(ppm)	0.1	0.1	0.1	0.1	0.1	0.3	0.3
Mo	(ppm)	21.1	28.1	29.3	78.9	136.3	81.7	69.8
Ni	(ppm)	3.9	4.5	8.6	8.2	7.7	8.8	9.3
Pb	(ppm)	18.2	19.5	26.6	49.9	56.3	49.5	36.2
Sb	(ppm)	3.6	4.6	7.1	33.1	35.0	24.4	16.7
Se	(ppm)	1.4	1.1	2.6	2.7	3.0	3.7	5.1
Te	(ppm)	0.5	0.5	0.8	1.9	2.5	2.1	1.5
Tl	(ppm)	0.7	0.6	0.5	0.6	0.4	0.3	0.1
Zn	(ppm)	139	130	111	112	83	71	36
Ba	(wt %)	0.30	0.31	0.41	1.68	2.67	1.73	1.25
Be	(ppm)	2.3	2.5	3.1	2.2	2.0	2.6	2.6
Cr	(ppm)	23	21	26	41	49	43	46
Cs	(ppm)	2.7	2.3	2.5	3.5	2.5	1.0	0.7
Ga	(ppm)	23.3	22.7	22.5	22.0	21.1	18.3	13.0
Hf	(ppm)	9.6	9.4	8.9	7.9	5.4	2.8	1.2
Li	(ppm)	11	13	15	17	16	10	8
Nb	(ppm)	31	32	45	62	87	141	191
Rb	(ppm)	221	197	152	94	54	28	8
Sc	(ppm)	3.3	3.4	3.4	4.1	3.5	3.4	2.7
Sn	(ppm)	8	10	13	28	41	40	40
Sr	(ppm)	136	146	192	362	520	450	242
Ta	(ppm)	3.1	2.8	3.1	2.6	2.0	2.2	1.5
Th	(ppm)	60	56	52	39	31	25	19
V	(ppm)	12	16	26	31	42	81	116
W	(ppm)	13	21	33	116	204	125	129
Y	(ppm)	47	50	57	60	71	73	79
Zr	(ppm)	318	312	289	258	173	83	45
La	(ppm)	0.03	0.04	0.06	0.10	0.15	0.15	0.12
Ce	(ppm)	0.05	0.06	0.09	0.15	0.21	0.22	0.17
Pr	(ppm)	46	57	81	127	178	188	159
Nd	(ppm)	125	154	213	322	440	481	437
Sm	(ppm)	16.2	18.5	24.4	33.4	43.3	48.9	43.6
Eu	(ppm)	4.6	5.0	6.4	12.6	16.5	15.8	14.0
Gd	(ppm)	12.7	14.0	17.5	22.2	28.5	26.8	29.0
Tb	(ppm)	1.7	1.9	2.3	2.7	3.5	3.2	3.5
Dy	(ppm)	9.4	10.1	11.7	13.1	16.9	15.4	16.2
Ho	(ppm)	1.8	1.9	2.2	2.3	3.1	2.8	3.0
Er	(ppm)	5.6	5.9	6.6	7.0	9.4	8.0	8.7
Tm	(ppm)	0.6	0.6	0.8	0.9	1.2	1.1	1.1
Yb	(ppm)	5.8	6.0	6.7	6.9	8.6	7.4	8.1
Lu	(ppm)	0.9	0.9	1.0	1.0	1.3	1.1	1.2

[1] Samples from the 10,000-sample MLA data set; all analyses conducted at AMDEL-Bureau Veritas, Adelaide

TABLE A4. Conditional Means Cu-Mineralized Samples[1]

		Mineralized samples (Cu ≥3,000 ppm)						
		< 5% Fe n = 180	5–10 % Fe n = 825	10–20% Fe n = 1414	20–30% Fe n = 1027	30–40% Fe n = 893	40–50% Fe n = 666	≥50% Fe n = 325
SiO_2	(wt %)	68.8	63.8	55.1	42.5	30.1	20.1	11.82
TiO_2	(wt %)	0.33	0.32	0.29	0.24	0.17	0.11	0.05
Al_2O_3	(wt %)	13.10	12.10	10.22	7.64	4.79	3.00	1.34
Fe_2O_3	(wt %)	5.90	10.8	20.9	35.7	49.8	63.9	77.1
MnO	(wt %)	0.03	0.08	0.13	0.14	0.14	0.19	0.22
MgO	(wt %)	0.29	0.35	0.43	0.43	0.34	0.40	0.39
CaO	(wt %)	0.50	1.05	1.49	1.90	2.52	1.97	1.31
Na_2O	(wt %)	0.17	0.17	0.13	0.10	0.09	0.07	0.07
K_2O	(wt %)	6.20	5.69	4.06	2.55	1.44	0.65	0.20
P_2O_5	(wt %)	0.07	0.12	0.23	0.35	0.38	0.54	0.54
CO_2	(wt %)	0.27	1.13	1.73	1.99	2.14	2.57	2.30
S	(wt %)	0.32	0.55	1.04	1.55	2.06	2.28	2.71
F	(wt %)	0.49	0.84	1.10	1.33	1.70	1.22	0.60
Cl	(ppm)	298	301	308	315	291	401	681
Cu	(ppm)	6995	7528	9975	12839	13664	15144	11354
U_3O_8	(ppm)	125	180	283	399	432	495	459
Au	(ppb)	119.9	222.6	397.6	622.7	652.3	578.9	332.5
Ag	(ppm)	1.7	1.8	2.0	2.4	2.7	2.7	2.0
As	(ppm)	37.1	46.3	96.0	175	272	132	86
Bi	(ppm)	2.8	4.2	6.0	6.8	8.6	6.6	4.8
Cd	(ppm)	0.4	0.5	0.8	0.4	0.4	0.2	0.1
Co	(ppm)	14.4	25.4	51.9	75.4	92.5	116.1	169.7
In	(ppm)	0.1	0.1	0.2	0.2	0.2	0.2	0.2
Mo	(ppm)	27.0	45.1	57.5	88.2	164.3	83.8	48.5
Ni	(ppm)	3.9	4.4	7.1	10.1	10.2	13.6	17.4
Pb	(ppm)	32.5	34.5	53.4	66.3	72.9	68.8	52.7
Sb	(ppm)	4.0	7.6	12.5	21.1	29.0	14.9	8.1
Se	(ppm)	2.2	1.5	3.3	5.2	6.0	8.7	9.6
Te	(ppm)	1.1	1.1	1.5	2.2	2.7	2.1	1.3
Tl	(ppm)	0.6	0.7	0.6	0.6	0.5	0.3	0.1
Zn	(ppm)	220	252	349	208	213	101	80
Ba	(wt %)	0.30	0.47	0.78	1.13	1.80	0.80	0.41
Be	(ppm)	2.0	2.1	2.6	2.9	2.7	2.9	2.6
Cr	(ppm)	18	20	25	32	32	33	34
Cs	(ppm)	2.7	2.6	2.6	2.4	1.5	0.8	0.4
Ga	(ppm)	23.9	24.0	24.5	24.6	22.7	19.2	14.4
Hf	(ppm)	9.7	9.4	8.3	6.6	4.6	2.6	1.0
Li	(ppm)	13	15	17	18	14	11	6
Nb	(ppm)	33	35	53	86	102	170	237
Rb	(ppm)	198	185	142	97	57	28	8
Sc	(ppm)	3.4	3.8	3.7	3.6	3.4	3.1	2.6
Sn	(ppm)	10	13	21	33	46	40	36
Sr	(ppm)	187	213	313	425	474	395	201
Ta	(ppm)	2.8	3.2	2.7	2.7	2.2	2.2	1.8
Th	(ppm)	61	56	50	42	30	23	19
V	(ppm)	13	15	21	30	32	41	60
W	(ppm)	20	37	68	123	272	138	79
Y	(ppm)	52	62	79	93	97	110	82
Zr	(ppm)	319	299	261	204	137	74	29
La	(ppm)	0.05	0.08	0.12	0.16	0.18	0.15	0.08
Ce	(ppm)	0.08	0.11	0.17	0.23	0.26	0.23	0.13
Pr	(ppm)	66	98	150	203	220	207	128
Nd	(ppm)	176	254	393	532	560	554	354
Sm	(ppm)	21.1	27.8	41.2	54.9	57.7	60.1	40.0
Eu	(ppm)	6.6	9.0	12.4	16.3	18.5	15.5	9.5
Gd	(ppm)	15.2	19.7	28.0	35.9	38.0	40.1	27.5
Tb	(ppm)	2.0	2.5	3.4	4.2	4.3	4.6	3.3
Dy	(ppm)	10.8	13.0	16.7	20.2	20.6	22.6	16.6
Ho	(ppm)	2.0	2.3	3.0	3.6	3.6	4.0	3.1
Er	(ppm)	6.3	7.4	9.1	10.6	10.8	12.0	9.4
Tm	(ppm)	0.7	0.9	1.2	1.4	1.4	1.6	1.3
Yb	(ppm)	6.5	7.3	8.6	9.8	10.2	10.9	8.9
Lu	(ppm)	1.0	1.1	1.3	1.4	1.5	1.6	1.4

[1] Samples from the 10,000-sample MLA data set; all analyses conducted at AMDEL-Bureau Veritas, Adelaide

View publication stats